

# The rotation of Io predicted by the Poincaré-Hough model

Benoît Noyelles<sup>1</sup>

*NAmur Center for Complex SYStems (NAXYS), FUNDP - University of Namur, Dpt of Mathematics, 8 Rempart de la Vierge, B-5000 Namur, Belgium*

## ABSTRACT

This paper proposes to study the rotation of the Galilean satellite of Jupiter Io, in considering core-mantle coupling. This satellite is particularly interesting because it experiences strong tidal dissipation inducing a very active surface. Moreover, the flow of the fluid inside its core is reputed to be unstable.

We first elaborate 10 different models of the interior of Io, considering either a Fe or a FeS core, using measured values of the gravity coefficients  $J_2$  and  $C_{22}$ , before studying their response to the 4-degrees of freedom Poincaré-Hough model. The study requires numerical methods like integration of ODE and frequency analysis of the solutions. We then study the stability of the flow of the fluid.

We show that these different models have a quite small influence on the longitudinal librations and the equilibrium obliquity, with amplitude of about 30 at 8 seconds of arc respectively, because of the relatively small inertia of the core. However, sulfur in the core can pump the tilt of the velocity field constituting the core. Moreover, in all our models the flow is unstable with a growth time of about 1,000 years for a Fe core and 5,000 years for a FeS one.

*Subject headings:* Io – Resonances, spin-orbit – Rotational dynamics – Interiors – Celestial mechanics

## 1. Introduction

Thanks to the Galileo space mission in the Jovian system, we have now interesting clues on Io's internal structure. In particular, its mass and its second-order gravity field parameters harmonics  $J_2$  and  $C_{22}$  are known with a good accuracy (Anderson et al. 2001).

---

<sup>1</sup>email: Benoit.Noyelles@fundp.ac.be, also associated with IMCCE, CNRS UMR 8028, Paris Observatory, UPMC, USTL, 77 avenue Denfert-Rochereau, 75014 Paris, France

Moreover, internal heating due to an intense tidal dissipation (Peale et al. 1979; Lainey et al. 2009) is expected to induce a fluid core (Cassen et al. 1982).

We recently published a theoretical exploration of the Poincaré-Hough model applied to a synchronously rotating body (Noyelles 2012). This model, originally proposed independently by (Hough 1895) and (Poincaré 1910) before being put on an Hamiltonian form by (Touma & Wisdom 2001), describes the rotational dynamics of a triaxial body composed of a rigid mantle and an ellipsoidal cavity filled by an inviscid fluid of constant uniform density and vorticity. This is a 4-degrees of freedom conservative model in which the core-mantle interactions result in pressure coupling at the core-mantle boundary.

This paper proposes an application of this model to a realistic Io, i.e. in considering the informations we dispose of to build internal models of Io that can be used by the Poincaré-Hough model, and in using complete orbital ephemerides, here from (Lainey et al. 2006), to take every forcing frequency into account. After computation of Io’s rotation we will discuss the problem of the elliptical instability of the fluid filling the core.

## 2. Modeling the interior

We here consider Io to be an ellipsoidal body, its moments of inertia being  $O < A \leq B \leq C$ .  $A$  is the moment of inertia with respect to Io’s long equatorial axis, while  $C$  is related to the polar axis. The core is ellipsoidal as well, its principal axes of inertia being collinear to the ones of the whole body, the moments associated being written  $A_c$ ,  $B_c$  and  $C_c$ .

The Poincaré-Hough model requires the following 5 parameters:

- Polar flattening  $\epsilon_1 = \frac{2C-A-B}{2C} = J_2 \frac{MR^2}{C}$ ,
- Equatorial ellipticity  $\epsilon_2 = \frac{B-A}{2C} = 2C_{22} \frac{MR^2}{C}$ ,
- Polar flattening of the core  $\epsilon_3 = \frac{2C_c-A_c-B_c}{2C_c}$ ,
- Equatorial ellipticity of the core  $\epsilon_4 = \frac{B_c-A_c}{2C_c}$ ,
- Relative inertia of the core  $\delta = \frac{C_c}{C}$ .

We here aim at determining these parameters from the known ones, particularly thanks to Galileo spacecraft. The known gravity and shape parameters of Io are gathered in Tab.1.

Table 1: Gravity and shape parameters of Io.

Quantity	Value	Reference
Mean density $\bar{\rho}$	$3,527.8 \pm 2.9 \text{ kg/m}^3$	Anderson et al. (2001)
$J_2$	$(1.8459 \pm 0.0042) \times 10^{-3}$	Anderson et al. (2001)
$C_{22}$	$(5.537 \pm 0.012) \times 10^{-4}$	Anderson et al. (2001)
$I/(MR^2)$	$0.37685 \pm 0.00035$	Anderson et al. (2001)
Mean radius R	1821.49 km	Archinal et al. (2011)
Subplanetary equatorial radius a	1,829.4 km	Archinal et al. (2011)
Along orbit equatorial radius b	1,819.4 km	Archinal et al. (2011)
Polar radius c	1,815.7 km	Archinal et al. (2011)

The value we take for the mean moment of inertia  $I = (A + B + C)/3$  is in fact attributed to the polar moment of inertia  $C$  in (Anderson et al. 2001). The authors obtain it from the following formula

$$\frac{C}{MR^2} \approx \frac{I}{MR^2} = \frac{2}{3} \left( 1 - \frac{2}{5} \sqrt{\frac{4 - k_2}{1 + k_2}} \right), \quad (1)$$

where  $M$  is the mass of Io, and  $k_2$  the second-degree potential Love number (see also (Van Hoolst et al. 2008) for more information on this formula). We have in fact from the definitions of  $J_2$  and  $I$ :

$$\frac{C}{MR^2} = \frac{I}{MR^2} + \frac{2}{3} J_2 = 0.37808. \quad (2)$$

We can see from these data that the 2 parameters  $\epsilon_1$  and  $\epsilon_2$  can be straightforwardly derived, yielding:

$$\begin{aligned} \epsilon_1 &= 4.88230 \times 10^{-3}, \\ \epsilon_2 &= 2.92901 \times 10^{-3}. \end{aligned}$$

We now explain how and under which assumptions we get the other parameters  $\epsilon_3$ ,  $\epsilon_4$  and  $\delta$ .

## 2.1. Obtaining the parameters

This study is inspired from the calculations of interior models of Mimas given in Noyelles et al. (2011). That study was different in the sense of Mimas' gravity coefficients  $J_2$  and  $C_{22}$  are

unknown and that its internal structure is assumed to be composed of two rigid layers of different porosities, but some calculations are same.

Let us consider the following parameters:

- $a_c, b_c, c_c$ : radii of the core, the principal axes being collinear to the ones corresponding to the dimensions of Io a, b and c,
- $\rho_c$ : constant density of the core,
- $\rho_m$ : constant density of the mantle,
- $R_c$ : mean radius of the core.

The knowledge of Io's mass gives a relation between  $\rho_c$  and  $\rho_m$ . From

$$\frac{4\pi}{3}\bar{\rho}R^3 = \frac{4\pi}{3}(\rho_c R_c^3 + \rho_m(R^3 - R_c^3)) \quad (3)$$

we get

$$R_c = R \left( \frac{\bar{\rho} - \rho_m}{\rho_c - \rho_m} \right)^{1/3}. \quad (4)$$

We can express the moment of inertia  $I$  with

$$\begin{aligned} \frac{I}{MR^2} &= \frac{\frac{8\pi}{15}(R_c^5 \rho_c + (R^5 - R_c^5) \rho_m)}{\frac{4\pi}{3}R^2(R_c^3 \rho_c + (R^3 - R_c^3) \rho_m)} \\ &= \frac{2}{5} \left( \frac{(\bar{\rho} - \rho_m)^{5/3}}{\rho(\rho_c - \rho_m)^{2/3}} + \frac{\rho_m}{\bar{\rho}} \right). \end{aligned} \quad (5)$$

Then, an assumption on  $\rho_c$  yields  $\rho_m$ .

We call  $(\vec{f}_1, \vec{f}_2, \vec{f}_3)$  the three unit vectors constituting the reference frame linked to the principal axes of inertia of Io, and  $(x, y, z)$  the coordinates of a point located inside the volume of Io. We have, from the definitions of the moments of inertia:

$$A_c = \iiint_{core} \rho_c (y^2 + z^2) dx dy dz, \quad (6)$$

$$B_c = \iiint_{core} \rho_c (x^2 + z^2) dx dy dz, \quad (7)$$

$$C_c = \iiint_{core} \rho_c (x^2 + y^2) dx dy dz, \quad (8)$$

$$\begin{aligned} A &= \iiint_{Io} \bar{\rho} (y^2 + z^2) dx dy dz \\ &= \iiint_{core} \rho_c (y^2 + z^2) dx dy dz + \iiint_{mantle} \rho_m (y^2 + z^2) dx dy dz, \end{aligned} \quad (9)$$

$$\begin{aligned} B &= \iiint_{Io} \bar{\rho} (x^2 + z^2) dx dy dz \\ &= \iiint_{core} \rho_c (x^2 + z^2) dx dy dz + \iiint_{mantle} \rho_m (x^2 + z^2) dx dy dz, \end{aligned} \quad (10)$$

$$\begin{aligned} C &= \iiint_{Io} \bar{\rho} (x^2 + y^2) dx dy dz \\ &= \iiint_{core} \rho_c (x^2 + y^2) dx dy dz + \iiint_{mantle} \rho_m (x^2 + y^2) dx dy dz, \end{aligned} \quad (11)$$

this yields

$$A_c = \frac{4\pi}{15} \rho_c a_c b_c c_c (b_c^2 + c_c^2), \quad (12)$$

$$B_c = \frac{4\pi}{15} \rho_c a_c b_c c_c (a_c^2 + c_c^2), \quad (13)$$

$$C_c = \frac{4\pi}{15} \rho_c a_c b_c c_c (a_c^2 + b_c^2), \quad (14)$$

$$A = \frac{4\pi}{15} (\rho_c a_c b_c c_c (b_c^2 + c_c^2) + \rho_m (abc (b^2 + c^2) - a_c b_c c_c (b_c^2 + c_c^2))), \quad (15)$$

$$B = \frac{4\pi}{15} (\rho_c a_c b_c c_c (a_c^2 + c_c^2) + \rho_m (abc (a^2 + c^2) - a_c b_c c_c (a_c^2 + c_c^2))), \quad (16)$$

$$C = \frac{4\pi}{15} (\rho_c a_c b_c c_c (a_c^2 + b_c^2) + \rho_m (abc (a^2 + b^2) - a_c b_c c_c (a_c^2 + b_c^2))). \quad (17)$$

$C$  is already known thanks to Eq.2, and we know  $A$  and  $B$  from the definitions of  $J_2$  and  $C_{22}$ , i.e.

$$A = 1.11149 \times 10^{20} \text{ kg.km}^2, \quad (18)$$

$$B = 1.11805 \times 10^{20} \text{ kg.km}^2, \quad (19)$$

$$C = 1.12024 \times 10^{20} \text{ kg.km}^2. \quad (20)$$

Then the radii of the core  $a_c$ ,  $b_c$  and  $c_c$  are deduced from the Eq.15 to 17, and the moments associated  $A_c$ ,  $B_c$  and  $C_c$  are given from the Eq.12 to 14. Finally the parameters required by the Poincaré-Hough model, i.e.  $\epsilon_3$ ,  $\epsilon_4$  and  $\delta$ , are straightforwardly derived.

## 2.2. 10 interior models

The presence of a large metallic core is an "inescapable conclusion" (Anderson et al. 1996) from Io's mean density and measurements of  $J_2$  and  $C_{22}$ , consistent with a differentiated body. Two compositions of the core are acceptable: either it is pure iron with a few nickel, its density being  $\rho_c \approx 8,000 \text{ kg/m}^3$ , either it is a close-to-eutectic mixture of iron and sulfur (with some nickel as well), with  $\rho_c \approx 5,150 \text{ kg/m}^3$  (Usselman 1975).

Another uncertainty is in the composition of the crust. Anderson et al. (2001) considered 2 possibilities: either a thin ( $\leq 50 \text{ km}$ ) crust with a low density ( $\leq 2,600 \text{ kg/m}^3$ ), or a small amount of low density crust (that we propose to neglect) overlying a thicker (100-200 km) melt-rich asthenosphere (density between 3,000 and 3,200  $\text{kg/m}^3$ ). The reader can find additional information on Io's internal structure in (de Pater & Lissauer 2010).

Considering a rigid crust in addition to the mantle does not really complexify the study since the system mantle+crust can be seen in the rotational model as a unique rigid layer. This requires to introduce the 3 outer radii of the mantle  $a_m$ ,  $b_m$  and  $c_m$ , its mean radius  $R_m$ , the density of the crust  $\rho_s$  (s standing for shell), and to complexify a little the formulae given above. We get in particular:

$$R_c = \left( \frac{R^3 (\rho - \rho_s) + R_m^3 (\rho_s - \rho_m)}{\rho_c - \rho_m} \right)^{1/3}, \quad (21)$$

$$\frac{I}{MR^2} = \frac{2}{5} \frac{\rho_c R_c^5 + \rho_m (R_m^5 - R_c^5) + \rho_s (R^5 - R_m^5)}{R^2}, \quad (22)$$

$$A = \frac{4\pi}{15} (\rho_c a_c b_c c_c (b_c^2 + c_c^2) + \rho_m (a_m b_m c_m (b_m^2 + c_m^2) - a_c b_c c_c (b_c^2 + c_c^2))) + \frac{4\pi}{15} \rho_s (a b c (b^2 + c^2) - a_m b_m c_m (b_m^2 + c_m^2)), \quad (23)$$

the moments of inertia  $B$  and  $C$  being obtained the same way.

From these putative internal structures we derived 10 interior models:

1. *Model 1*: 2 layers, liquid core made of pure iron (Fe) + homogeneous mantle,
2. *Model 2*: 2 layers, liquid core made of an eutectic mixture of iron and sulfur (FeS) + homogeneous mantle,
3. *Model 3*: 3 layers, core Fe, crust of constant thickness (30 km) with  $\rho_s = 2,400\text{kg}/\text{m}^3$ ,
4. *Model 4*: 3 layers, core FeS, crust of constant thickness (30 km) with  $\rho_s = 2,400\text{kg}/\text{m}^3$ ,
5. *Model 5*: 3 layers, core Fe, crust homothetical to the shape of Io, of mean thickness =30 km with  $\rho_s = 2,400\text{kg}/\text{m}^3$ ,
6. *Model 6*: 3 layers, core FeS, crust homothetical to the shape of Io, of mean thickness =30 km with  $\rho_s = 2,400\text{kg}/\text{m}^3$ ,
7. *Model 7*: 3 layers, core Fe, crust of constant thickness (150 km) with  $\rho_s = 3,100\text{kg}/\text{m}^3$ ,
8. *Model 8*: 3 layers, core FeS, crust of constant thickness (150 km) with  $\rho_s = 3,100\text{kg}/\text{m}^3$ ,
9. *Model 9*: 3 layers, core Fe, crust homothetical to the shape of Io, of mean thickness =150 km with  $\rho_s = 3,100\text{kg}/\text{m}^3$ ,
10. *Model 10*: 3 layers, core FeS, crust homothetical to the shape of Io, of mean thickness =150 km with  $\rho_s = 3,100\text{kg}/\text{m}^3$ .

The parameters related to the internal structures of these 10 models are gathered in Tab.2, while their conversion into Poincaré-Hough parameters are given in Tab.3.

We can see that the 10 models can be splitted into 2 groups, the discrimination coming from the composition of the core. If the core is made of pure iron, its radius is  $\approx 650$  km, while it reaches  $\approx 930$  km if made of a eutectic mixture of iron and sulfur. These numbers are consistent with the upper bounds of radii given in (Anderson et al. 2001), i.e. 300 to 650 km for a pure iron core, and 550 to 900 km for a FeS core. Another notable point is that the polar radius of the core is not the smallest one. This is a priori unexpected and somehow contradicts an assumption expressed in (Noyelles 2012), i.e.  $0 < A_c \leq B_c \leq C_c$ . But this assumption is in fact not used in the calculations, the real constraint of this model being that the principal axes of inertia of the core are collinear to the ones of the whole body.

Table 2: Physical parameters of our 10 models.

Models	$\rho_c$ ( $kg/m^3$ )	$\rho_m$ ( $kg/m^3$ )	$\rho_s$ ( $kg/m^3$ )	$a_c$ ( $km$ )	$b_c$ ( $km$ )	$c_c$ ( $km$ )	$R_c$ ( $km$ )
1	8,000	3,291.465	–	690.411	660.545	663.908	671.904
3	8,000	3,377.242	2,400	657.994	623.714	629.205	635.355
5	8,000	3,377.250	2,400	659.698	623.277	627.958	365.355
7	8,000	3,409.044	3,100	650.283	614.596	620.705	628.935
9	8,000	3,409.044	3,100	652.451	614.040	619.119	628.935
2	5,150	3,243.815	–	978.846	958.372	959.124	965.144
4	5,150	3,337.988	2,400	936.963	913.946	915.956	922.517
6	5,150	3,337.988	2,400	937.918	913.696	915.256	922.517
8	5,150	3,351.865	3,100	936.495	913.320	915.379	921.963
10	5,150	3,351.865	3,100	937.477	913.064	914.660	921.963

Usually, interior models are made in solving Clairaut’s differential equation (Jeffreys 1976; Van Hoolst et al. 2008) to get the flattening  $\alpha$  at any mean radius  $r_0$ , assuming hydrostatic equilibrium in the whole body. This yields

$$\frac{d^2\alpha}{dr_0^2} + \frac{6}{r_0} \frac{\rho}{\bar{\rho}} \frac{d\alpha}{dr_0} - \frac{6}{r_0^2} \left(1 - \frac{\rho}{\bar{\rho}}\right) \alpha = 0, \quad (24)$$

where  $\bar{\rho}$  is the mean density of the sphere of radius  $r_0$ , and

$$\alpha = \frac{a + b - 2c}{a + b}. \quad (25)$$

Here the value of  $I$  uses the assumption of the hydrostatic equilibrium on the whole body, and this allows us to get 3 equations yielding  $a_c$ ,  $b_c$  and  $c_c$ . That is the reason why we do not use Clairaut’s equation. We prefer in fact to use measured values of  $J_2$  and  $C_{22}$  instead of estimating them from tidal and rotational deformation. Anyway, getting  $b_c < c_c$  is puzzling. This could be due to the assumption of constant densities of the layers and collinearity of their principal axes of inertia.

As expected, the parameters required by the Poincaré-Hough model result in 2 groups as well, due to the composition of the core. We can note the small values of  $\delta$ , that seem to be very small in comparison with Mercury ( $\delta > 0.39$  according to Margot et al. (2007)), but are closer to the Moon’s as given by (Williams et al. 2001), where  $\delta$  lies between  $7.3 \times 10^{-4}$  and  $1.08 \times 10^{-3}$ . Moreover, we can see important numbers for the ratio  $\epsilon_4/\epsilon_2$ , this is due to the unexpected small value of  $b_c$ .

Table 3: Parameters required by the Poincaré-Hough model.

Models	$\epsilon_1$ $\times 1000$	$\epsilon_2$ $\times 1000$	$\epsilon_3$ $\times 100$	$\epsilon_4$ $\times 100$	$\delta$ $\times 100$	$\epsilon_3/\epsilon_1$	$\epsilon_4/\epsilon_2$
1	4.882	2.929	1.722	2.210	1.654	3.527	7.544
3	4.882	2.929	1.836	2.673	1.270	3.760	9.125
5	4.882	2.929	2.125	2.837	1.272	4.353	9.684
7	4.882	2.929	1.877	2.819	1.188	3.844	9.625
9	4.882	2.929	2.250	3.030	1.191	4.608	10.345
2	4.882	2.929	0.980	1.057	6.503	2.007	3.608
4	4.882	2.929	1.029	1.243	5.175	2.107	4.245
6	4.882	2.929	1.142	1.308	5.179	2.338	4.455
8	4.882	2.929	1.033	1.253	5.160	2.115	4.277
10	4.882	2.929	1.149	1.319	5.164	2.353	4.503

### 3. The rotational dynamics

In all the calculations, the rotational dynamics of Io is assumed to be influenced by the gravitational torque of its parent planet, i.e. Jupiter, responsible for the spin-orbit resonance. For that, we need to model the position of Jupiter with respect to Io at any time. We used L1.2 ephemeris (Lainey et al. 2006) that consider perturbations of the orbit of Io by a flattened Jupiter, the other Galilean satellites and the Sun. Including complete ephemeris allows to consider any sinusoidal perturbation likely to influence the rotational outputs. After a description of Io’s orbital dynamics, we present our rotational model.

#### 3.1. Orbital dynamics of Io

The system of the 4 Galilean satellites of Jupiter, i.e. from J-1 Io to J-4 Callisto, has an interesting dynamical configuration. It involves a 3-body mean motion resonance, known as the Laplacian resonance, between Io, Europa, and Ganymede, of resonant argument  $\lambda_1 - 3\lambda_2 + 2\lambda_3$ ,  $\lambda_i$  being the mean longitude of the satellite J-i. Moreover, Io and Europa are close to the 2:1 mean motion resonance, as are Europa and Ganymede as well. This induces strong orbital perturbations likely to have consequences on the rotational dynamics. The effects on the keplerian orbital elements are shown in Fig.1.

We see in particular that the semimajor axis has an amplitude of variation larger than 30 km, and varies over a short timescale (a few days), as for the eccentricity. The orbital inclination with respect to Saturn’s equatorial plane is smaller than 3 arcmin, and

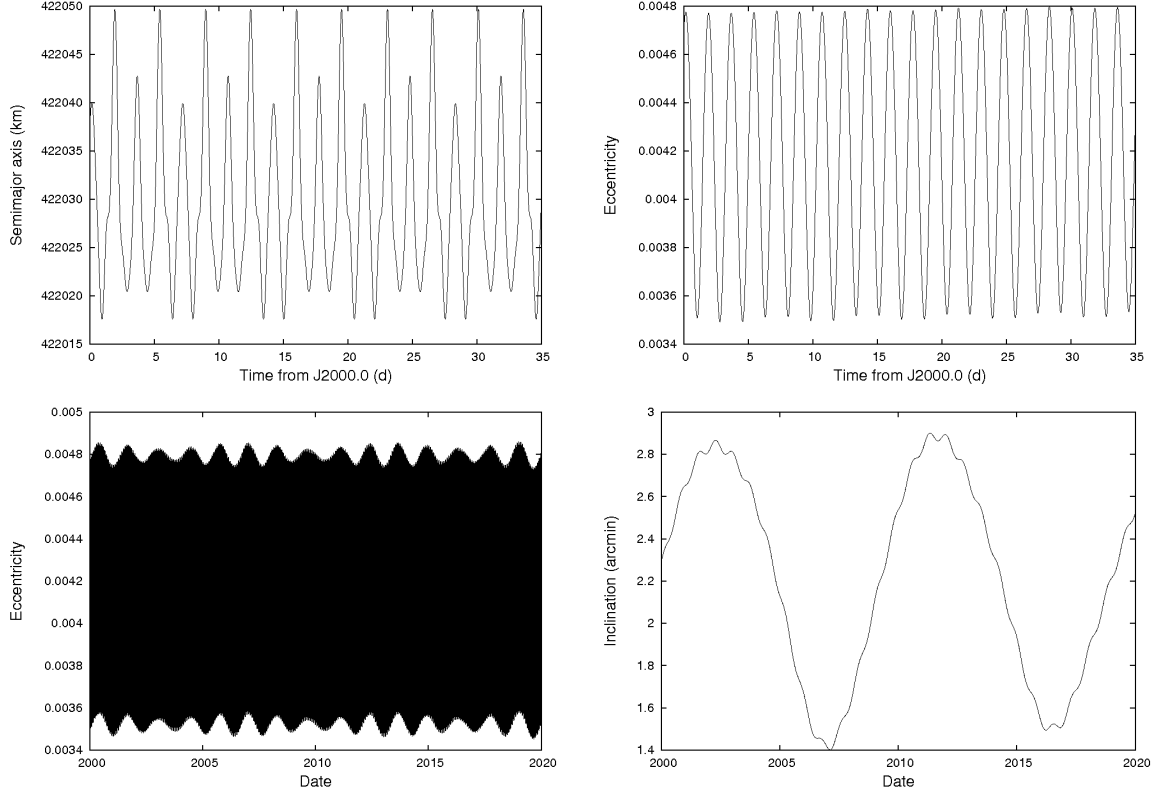


Fig. 1.— Variations of the keplerian elements of Io, as given by the theory L1.2 Lainey et al. (2006).

exhibits variations over a longer timescale (a few years). These variations can be given under quasiperiodic representations, i.e. infinite sums of trigonometric series based on a finite number of sinusoidal proper modes. These modes have been identified by Lainey et al. (2006) and are gathered in Tab.4. The notations with bullets are used to recall that the proper modes are close to keplerian elements ( $\lambda_i$  standing for the mean longitude of the satellite J-i,  $\varpi_i$  for the longitude of its pericenter, and  $\Omega_i$  of its ascending node), but are not exactly the same, since the orbital angles are not sinusoidal but just quasiperiodic. There should a priori be 12 proper modes, i.e. 3 due to each of the 4 satellites, while 17 are given here. In fact,  $\lambda_{\odot}^{\bullet}$  and  $\Omega_{\odot}^{\bullet}$  come from the contribution of the Sun, and we also have relations between the other proper modes, i.e.  $\lambda_1^{\bullet} - 3\lambda_2^{\bullet} + 2\lambda_3^{\bullet} = \pi$  (Laplacian resonance),  $\nu^{\bullet} = \lambda_1^{\bullet} - 2\lambda_2^{\bullet}$ , and  $\rho^{\bullet} = 3\lambda_3^{\bullet} - 7\lambda_4^{\bullet}$  (De Haerdtl inequality, see (De Haerdtl 1892; Lieske 1973; Noyelles & Vienne 2007)). Finally,  $\psi^{\bullet}$  is the proper mode resulting from the Laplacian resonance.

Table 4: Proper modes of the orbital dynamics of the Galilean satellites of Jupiter, given by Lainey et al. (2006). With all these modes, the orbits of the Galilean satellites can be reconstructed. The phases are given at J2000.0=JD 2451545.

Fundamental argument	Frequency (rad/year)	Phase (deg)	Period (day)	Period (year)
$\lambda_1^\bullet$	1,297.204472527975	19.933985	1.769	0.005
$\lambda_2^\bullet$	646.245120237676	−145.505456	3.551	0.010
$\lambda_3^\bullet$	320.765444090882	−138.224679	7.154	0.019
$\lambda_4^\bullet$	137.511596761768	80.963400	16.689	0.046
$\lambda_{\odot}^\bullet$	0.529679614322	36.023357	4,332.938	11.863
$\psi^\bullet$	1.114249427448	61.409022	2,059.622	5.639
$\nu^\bullet$	4.714232129692	−49.056046	486.809	1.333
$\rho^\bullet$	−0.284844595500	98.583494	8,056.791	22.058
$\varpi_1^\bullet$	0.973118537914	−66.931981	2,358.328	6.457
$\varpi_2^\bullet$	0.247629795307	146.599043	9,267.598	25.373
$\varpi_3^\bullet$	0.046486875982	−105.035305	49,367.340	135.160
$\varpi_4^\bullet$	0.011711777410	−6.531104	195,950.909	536.484
$\Omega_1^\bullet$	−0.845588849794	−102.210438	2,714.006	7.431
$\Omega_2^\bullet$	−0.207902639426	−175.568039	11,038.500	30.222
$\Omega_3^\bullet$	−0.045624499183	60.484939	50,300.463	137.715
$\Omega_4^\bullet$	−0.011162498389	−49.797856	205,593.170	562.883
$\Omega_{\odot}^\bullet$	0	138.277188	$\infty$	$\infty$

### 3.2. Numerical treatment of the rotation

Our rotational model is the same as in (Noyelles 2012), i.e. a 4-d.o.f. conservative model taking the pressure coupling at the core-mantle boundary into account. The Hamiltonian of the problem reads

$$\mathcal{H}(p, P, r, R, \xi_1, \eta_1, \xi_2, \eta_2) = \mathcal{H}_1(P, \xi_1, \eta_1, \xi_2, \eta_2) + \mathcal{H}_2(p, P, r, R, \xi_1, \eta_1), \quad (26)$$

where  $\mathcal{H}_1$  is the kinetic energy of the system, and  $\mathcal{H}_2$  the perturbing potential of Jupiter.

We have (see A)

$$\begin{aligned}
\mathcal{H}_1 = & \frac{n}{2(1-\delta)} \left( P^2 + \frac{P_c^2}{\delta} + 2\sqrt{\left(P - \frac{\xi_1^2 + \eta_1^2}{4}\right)\left(P_c - \frac{\xi_2^2 + \eta_2^2}{4}\right)} (\eta_1\eta_2 - \xi_1\xi_2) \right. \\
& \left. + 2\left(P - \frac{\xi_1^2 + \eta_1^2}{2}\right)\left(\frac{\xi_2^2 + \eta_2^2}{2} - P_c\right) \right) \\
& + \frac{n\epsilon_1}{2(1-\delta)^2} \left( P_c^2 - \left(\frac{\xi_2^2 + \eta_2^2}{2} - P_c\right)^2 + P^2 - \left(P - \frac{\xi_1^2 + \eta_1^2}{2}\right)^2 \right. \\
& \left. + 2\sqrt{\left(P - \frac{\xi_1^2 + \eta_1^2}{4}\right)\left(P_c - \frac{\xi_2^2 + \eta_2^2}{4}\right)} (\eta_1\eta_2 - \xi_1\xi_2) \right) \\
& + \frac{n\epsilon_2}{2(1-\delta)^2} \left( \frac{1}{4}(4P - \xi_1^2 - \eta_1^2)(\xi_1^2 - \eta_1^2) + \frac{1}{4}(4P_c - \xi_2^2 - \eta_2^2)(\xi_2^2 - \eta_2^2) \right. \\
& \left. - 2\sqrt{\left(P - \frac{\xi_1^2 + \eta_1^2}{4}\right)\left(P_c - \frac{\xi_2^2 + \eta_2^2}{4}\right)} (\eta_1\eta_2 + \xi_1\xi_2) \right) \\
& - \frac{n\epsilon_3}{2(1-\delta)^2} \left( \delta\left(P^2 - \left(P - \frac{\xi_1^2 + \eta_1^2}{2}\right)^2\right) + \left(P_c^2 - \left(\frac{\xi_2^2 + \eta_2^2}{2} - P_c\right)^2\right)\left(2 - \frac{1}{\delta}\right) \right. \\
& \left. + 2\delta\sqrt{\left(P - \frac{\xi_1^2 + \eta_1^2}{4}\right)\left(P_c - \frac{\xi_2^2 + \eta_2^2}{4}\right)} (\eta_1\eta_2 - \xi_1\xi_2) \right) \\
& + \frac{n\epsilon_4}{2(1-\delta)^2} \left( \frac{\delta}{4}(4P - \xi_1^2 - \eta_1^2)(\eta_1^2 - \xi_1^2) + \left(2 - \frac{1}{\delta}\right)\frac{1}{4}(4P_c - \xi_2^2 - \eta_2^2)(\eta_2^2 - \xi_2^2) \right. \\
& \left. + 2\delta\sqrt{\left(P - \frac{\xi_1^2 + \eta_1^2}{4}\right)\left(P_c - \frac{\xi_2^2 + \eta_2^2}{4}\right)} (\eta_1\eta_2 + \xi_1\xi_2) \right), \tag{27}
\end{aligned}$$

and

$$\mathcal{H}_2(p, P, r, R, \xi_1, \eta_1) = -\frac{3}{2} \frac{\mathcal{G}M_{\text{Jup}}}{nd^3} (\epsilon_1(x^2 + y^2) + \epsilon_2(x^2 - y^2)), \tag{28}$$

where  $\mathcal{G}$  is the gravitational constant,  $M_{\text{Jup}}$  the mass of Jupiter, and  $d$  the distance Io-Jupiter.  $x$ ,  $y$  and  $z$  are the coordinates of the vector pointing to Jupiter in the reference frame  $(\vec{f}_1, \vec{f}_2, \vec{f}_3)$  linked to the principal axes of inertia of Io.

In fact, a complete treatment of the problem requires to define 4 reference frames (Fig.2 & 3):

1.  $(\vec{e}_1, \vec{e}_2, \vec{e}_3)$ : inertial reference frame, in which the planetary ephemerides are given (here

the J2000 Jovian equatorial frame)

2.  $(\vec{n}_1^c, \vec{n}_2^c, \vec{n}_3^c)$ : linked to the angular momentum of the pseudo-core (see A). The Euler angles  $(h_c, K_c, g_c)$  position the vector  $\vec{n}_2^c$  on the plane perpendicular to the angular momentum of the pseudo-core.
3.  $(\vec{n}_1^c, \vec{n}_2^c, \vec{n}_3^c)$ : linked to the angular momentum of Io. The Euler angles  $(h, K, g)$  position the vector  $\vec{n}_2$  on the plane perpendicular to the angular momentum.
4.  $(\vec{f}_1, \vec{f}_2, \vec{f}_3)$ : linked to the principal axes of inertia of the satellite. The angles  $(l, J)$  and  $(l_c, J_c)$  position the axis of least inertia.

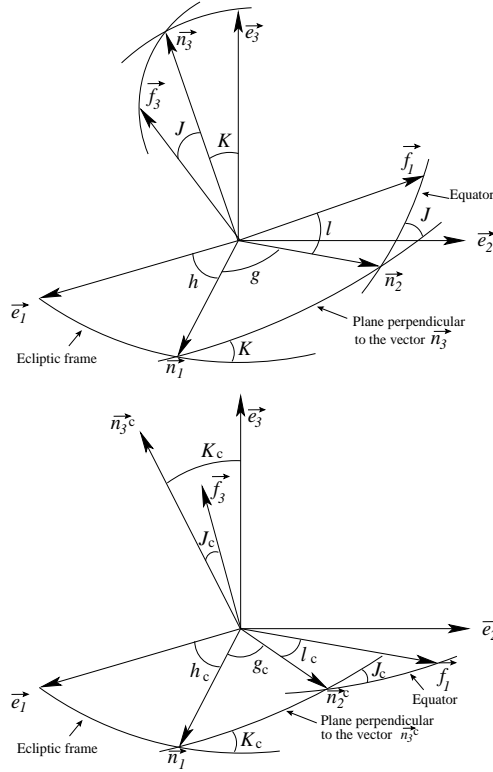


Fig. 2.— In the upper panel we have 3 reference frames: one linked to the ecliptic plane ( $\vec{e}_1, \vec{e}_2, \vec{e}_3$ ), another linked to the angular momentum  $\vec{G}$  ( $\vec{n}_1, \vec{n}_2, \vec{n}_3$ ), and the last one linked to the axes of inertia ( $\vec{f}_1, \vec{f}_2, \vec{f}_3$ ) of the satellite. In the lower panel we have a similar configuration but instead of the angular momentum of the satellite, we have a reference frame linked to the angular momentum of a pseudo-core

The canonical variables of the problem are:

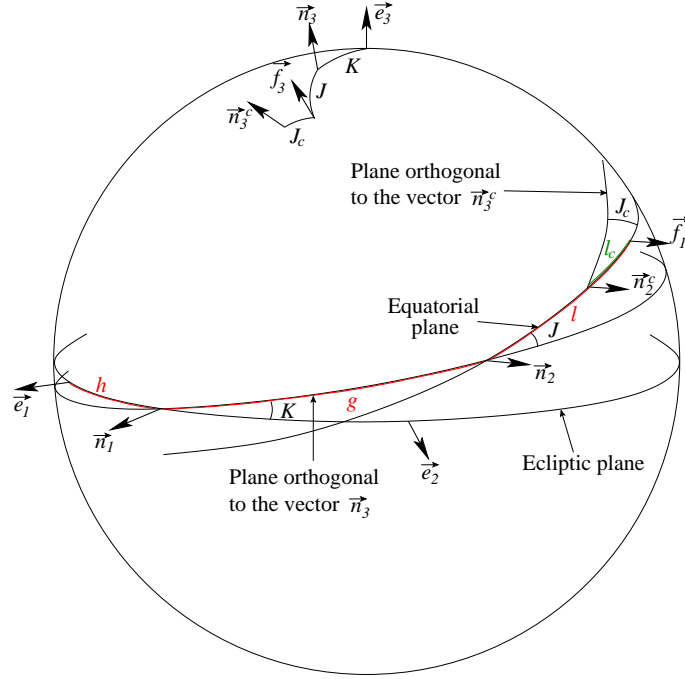


Fig. 3.— The four reference frames gathered in the same view. The angles  $(h, K)$  position the plane orthogonal to the angular momentum  $\vec{N}$ . The Euler angles  $(g, J, l)$  locate the axis of least inertia and the body frame  $(\vec{f}_1, \vec{f}_2, \vec{f}_3)$ . The angles  $(J_c, l_c)$  place the angular momentum of the pseudo-core with respect to the axis of least inertia  $\vec{f}_1$ .

$$\begin{aligned}
p &= l + g + h, & P &= \frac{G}{nC}, \\
r &= -h, & R &= P(1 - \cos K), \\
\xi_1 &= -\sqrt{2P(1 - \cos J)} \sin l, & \eta_1 &= \sqrt{2P(1 - \cos J)} \cos l, \\
\xi_2 &= \sqrt{2P_c(1 + \cos J_c)} \sin l_c, & \eta_2 &= \sqrt{2P_c(1 + \cos J_c)} \cos l_c,
\end{aligned} \tag{29}$$

where  $\vec{G}$  is the angular momentum of Io,  $P_c = G_c/(nC)$  where  $\vec{G}_c$  is the angular momentum of the pseudo-core, and  $l, g, h, K$  (obliquity of Io),  $J$  (amplitude of the polar motion) and  $J_c$  are Euler angles defined in the Fig.2 & 3.  $P_c$  is assumed to be constant and set to  $\delta = C_c/C$ , i.e. the ratio between the polar inertial momentum of the core and of the satellite. Because of the spin-orbit resonance, we should have  $G \approx nC$ , and the fluid inside the core is expected to follow the mantle on average, this yields  $G_c \approx nC_c$ . These variables are inspired from the modified Andoyer variables (Andoyer 1926).

From the Hamiltonian  $\mathcal{H}$  we derive the Hamilton equations:

$$\begin{aligned}
p, & & P, \\
r, & & R, \\
\xi_1, & & \eta_1, \\
\xi_2, & & \eta_2,
\end{aligned} \tag{30}$$

that we integrate numerically using the  $10^{th}$  predictor-corrector Adams-Bashforth-Moulton integrator.

The initial conditions are chosen in assuming that Io is at the Cassini State 1. This is a stable dynamical equilibrium that the system should have reached thanks to slow dissipations acting over the ages. The validity of this assumption is proved for instance in (Gladman et al. 1996). It consists of

- Io is at the 1:1 spin-orbit resonance. As a consequence, the angle  $\sigma = p - \lambda_1$  where  $\lambda_1$  is the mean longitude of Io is a resonant argument librating around 0 (or  $\pi$ ) with a small amplitude,
- the angle  $\rho = \varpi_1 + r$  where  $\varpi_1$  is the ascending orbital node of Io is librating with a small amplitude. This is a consequence of the Third Cassini Law, stating that the spin axis and the normals to the reference and orbital planes remain coplanar (Cassini 1693; Colombo 1966).

These laws have been extended by Bouquillon et al. (2003) who showed that the amplitude of the polar motion,  $J$ , should be small but not null. As a consequence,  $\xi_1$  and  $\eta_1$

are expected to be small. We also expect the tilt of the fluid to be small, i.e. we should have small  $\xi_2$  and  $\eta_2$ . In doing this, we are close to the actual equilibrium but not at its exact location. This yields free librations of the system around the equilibrium, with small amplitudes.

In fact, in a complexified system for instance considering the full orbital dynamics of Io, an exact analytical derivation of the equilibrium is hopeless without hard work. We bypass this problem in applying the numerical iterative algorithm NAFFO (Numerical Algorithm For Fundamental Frequencies, Noyelles et al. (2012)), consisting of 3 steps:

1. Numerical integration of the equations of the system, with quite good initial conditions derived from the definition of the Cassini State 1 (see above).
2. Quasiperiodic decompositions of the outputs describing the trajectory, and identification of the free librations.
3. Removal of the free librations from the initial conditions. This way, the initial conditions are improved and can be used in a new numerical integrations.

The process is iterated until convergence. (Noyelles et al. 2012) have shown that in a Hamiltonian framework, the amplitude is quadratic in the amplitude of the free librations. The quasiperiodic decompositions are made using an algorithm of frequency analysis inspired from Laskar’s NAFF (Laskar (1993, 2005), App.B). The basic idea is that, for a non-chaotic trajectory, every complex output  $x(t)$ , that are in fact our canonical variables, can be written as a quasiperiodic function of time as

$$x(t) = \sum_{n=0}^{\infty} A_n \exp(\imath \nu_n t), \quad (31)$$

where  $A_n$  are constant complex amplitudes and  $\nu_n$  constant frequencies. The algorithm of frequency analysis gives finite series such as

$$x(t) \approx \sum_{n=0}^N A_n^{\bullet} \exp(\imath \nu_n^{\bullet} t), \quad (32)$$

the bullet meaning that the amplitudes and frequencies have been numerically determined. In the case of a real variable, the Eq.32 becomes

$$x(t) \approx \sum_{n=0}^N A_n^{\bullet} \cos(\nu_n^{\bullet} t + \phi_n^{\bullet}), \quad (33)$$

or

$$x(t) \approx \sum_{n=0}^N A_n^{\bullet} \sin(\nu_n^{\bullet} t + \phi_n^{\bullet}), \quad (34)$$

where the amplitudes are now real, and the  $\phi_n^{\bullet}$  are real phases expressed with the counter-clockwise convention, previously included in the complex amplitudes in Eq.32. The numerical decompositions of the solutions into quasiperiodic series can be splitted into two parts: one called the *forced solution*, containing only frequencies coming from the orbital ephemerides, gathered in Tab.4, and the *free solution*, due to the departure of the initial conditions from the exact Cassini State 1, that contains the *proper* or *free* frequencies of the rotational dynamics. Since the rotational model has four degrees of freedom, we have four independent proper frequencies.

Once the numerical solution corresponding to the Cassini State 1 has been obtained, we convert it into observable outputs and perform frequency analysis to extract and identify the different contributions composing it.

## 4. Results

We here give the results of our numerical computations of Io’s rotational motion. We first show the values of the free frequencies in the 10 models, then we express the consequences on the observable rotation.

### 4.1. The proper (or free) frequencies

As said in the previous section, four independent proper frequencies coming from the free librations of the system around the equilibrium can be extracted from the solutions. The amplitudes associated are a priori expected to be too small to be detected, but knowing them allows to characterize the way the system reacts to any external sinusoidal sollicitation. If the frequency of the excitation is close to a proper frequency, the amplitude of response will be raised. It is for instance expected for Mercury, where the frequency of the free longitudinal librations ( $\approx 12$  years) is close to the period of the excitation by Jupiter, i.e. 11.86 years (Dufey et al. 2008; Peale et al. 2009; Yseboodt et al. 2010).

From a strictly mathematical point of view, these four proper modes are due to all the interactions involved in the system and can be found in any output. However, a physical

meaning can be given to them with a good approximation. These proper modes are

1.  $u$ : close to the free longitudinal librations.
2.  $v$ : close to the free librations of the obliquity.
3.  $w$ : close to the free polar motion, also designated as *wobble*.
4.  $z$ : close to the free motion of the velocity field of the fluid, also designated as *free core nutation* or *FCN*.

The frequencies of these proper modes are numerically determined by frequency analysis of the resonant argument  $\sigma = p - \lambda$  for  $u$ , of  $\rho = \varpi + r$  for  $v$ , of  $\eta_1 + \imath\xi_1$  for the wobble  $w$  and of  $\eta_2 + \imath\xi_2$  for the free core nutation  $z$ . The frequencies obtained are given in Tab.5.

Table 5: Free or proper frequencies  $\omega$  and the periods associated  $T$  for the 10 models of Io.

Models	$\omega_u$ (rad/yr)	$\omega_v$ (rad/yr)	$\omega_w$ (rad/yr)	$\omega_z$ (rad/yr)	$T_u$ (d)	$T_v$ (d)	$T_w$ (d)	$T_z$ (d)
1	173.4360	13.7957	10.1955	1,320.3243	13.2322	166.3520	225.0927	1.7382
3	173.0985	13.9452	10.1661	1,321.3757	13.2580	164.5679	225.7442	1.7368
5	173.1007	14.0594	10.1856	1,325.0328	13.2578	163.2318	225.3111	1.7320
7	173.0269	13.9763	10.1622	1,321.7963	13.2634	164.2023	225.8303	1.7362
9	173.0296	14.0844	10.2147	1,326.5235	13.2632	162.9420	224.6689	1.7300
2	177.8768	17.9647	10.7253	1,308.0619	12.9018	127.7468	213.9738	1.7545
4	176.6271	18.9578	10.5770	1,308.6329	12.9931	121.0550	216.9747	1.7537
6	176.6308	18.4342	10.5762	1,309.3529	12.9928	124.4933	216.9903	1.7527
8	176.6128	18.9880	10.5752	1,308.6631	12.9942	120.8621	217.0118	1.7536
10	176.6165	18.4817	10.5744	1,309.3957	12.9939	124.1734	217.0271	1.7527

As for the parameters  $\epsilon_i$  and  $\delta$ , the results can be splitted into two groups: the "odd" models, considering a core made of pure iron, and the "even" ones, assuming that the core contains sulfur. We can see that, because of the small value of  $\delta = C_c/C$ , the period of the free longitudinal librations is close to the one considering a rigid Io (13.25 days for Henrard (2005) with a slightly different gravity field, 13.31 days for Noyelles (2008) with quite the same as this paper, the only difference being the approximation  $C \approx I$ ). There exists an accurate analytical formula for this quantity (Goldreich & Peale 1966), in neglecting the core-mantle interactions:

$$T_u = \frac{\pi}{n} \sqrt{\frac{C/(MR^2)}{3C_{22}}} + O(e^2) = \sqrt{1 - \delta} T_{ur}, \quad (35)$$

where  $T_{ur}$  is the period of the longitudinal librations for a rigid Io ( $C_m = C$ ), i.e. 13.31 days in our case. This yields, for the cases 1 and 2 respectively, i.e. with  $\delta = 1.654 \times 10^{-2}$  and  $\delta = 6.503 \times 10^{-2}$ ,  $T_u = 13.20$  and  $T_u = 12.87$  days. We can also see that the frequency of the free core nutation  $\omega_z$  is close to the orbital frequency  $n = 1,297.20447$  rad/y (Tab.4) in particular for the "even" models, where  $\epsilon_3$  is smaller than for the other cases. This link between  $\epsilon_3$  and the proximity of  $\omega_z$  and  $n$  has already been highlighted in (Noyelles 2012). We can also see an influence of the composition of the core on the other two free frequencies  $\omega_v$  and  $\omega_w$ .

## 4.2. Observable outputs

Our canonical variables are very convenient for a mathematical analysis of the problem, but cannot be directly observed, in particular because 3 degrees of freedom refer to the whole Io and one to the pseudo-core, while only the mantle, i.e. the surface, can be observed. Moreover, if the core could be observed, it would be anyway different from the pseudo-core at the second order in its asphericity. That is the reason why we choose to express observable outputs, i.e.

- longitudinal librations of the mantle  $\phi_m = p_m - nt$ , where  $p_m$  is the spin angle of the mantle. Because of the spin-orbit resonance,  $nt$  is the slope of  $p_m$ , thus  $\phi_m$  is librating around a constant quantity that we set to 0 by a convenient choice of the longitude definition origin.
- obliquity of the mantle  $\epsilon_m$  (angle between the angular momentum of the mantle  $\vec{N}_m$  (Eq.A10) and the normal to the orbit of Io,
- amplitude of the polar motion  $J_m$ ,
- tilt of the velocity field of the fluid  $J_c$ .

The formulae giving these quantities are extensively derived in (Noyelles et al. 2010), Sect.4.1.

The Fig.4 shows these outputs for the Model 1 (iron core), over 50 years, and quasiperiodic decompositions of these quantities are given in Tab.6 to 9. The first plot gives the longitudinal librations and exhibits quite large variations of the amplitude of these librations over decades. As shown in Tab.6, at least 3 timescales should be considered:

1. Short-period librations ( $\approx 1.7$  d), that appear as the thickness of the line in Fig.4,
2.  $\approx 460$  d librations, that have the main amplitude and are due to the proximity of Io to the 2 : 1 mean motion resonance with Europa,
3.  $\approx 5.6$  y librations, signature of the Laplacian resonance.

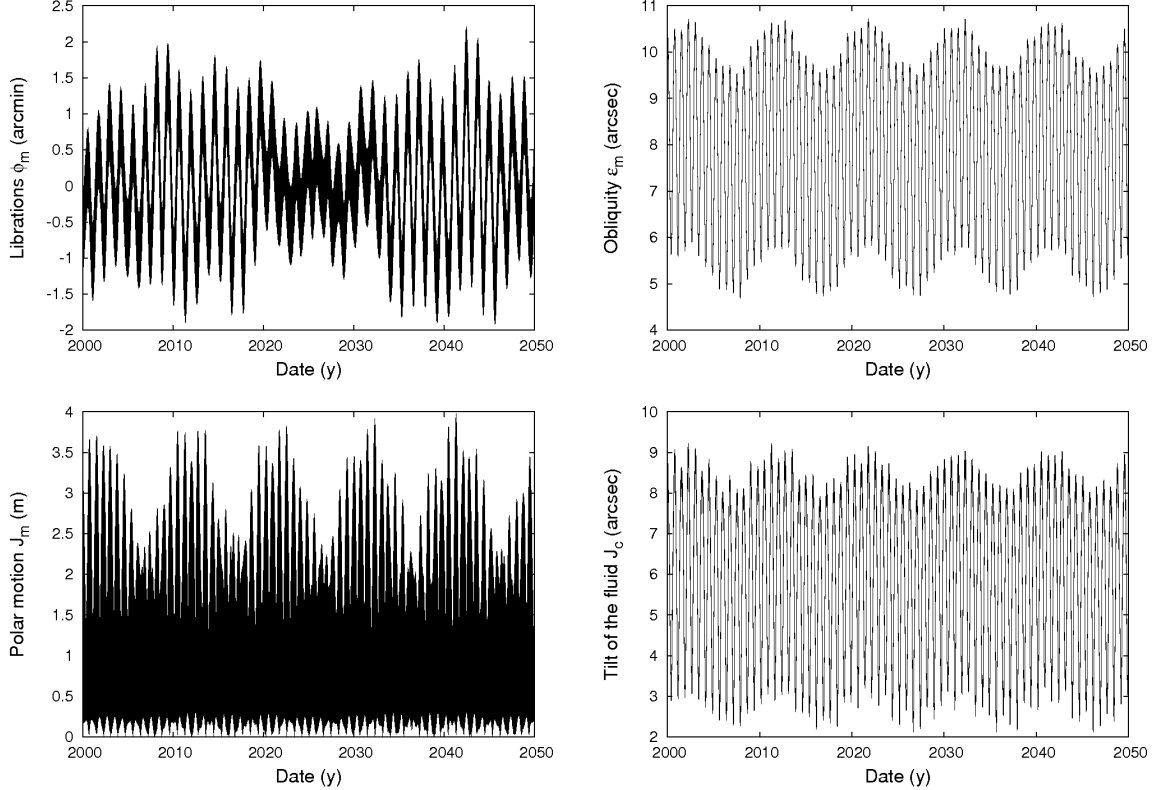


Fig. 4.— Observable outputs of the Model 1 (core made of pure iron).

The obliquity  $\epsilon_m$  (Fig.4 & Tab.7) is smaller than 11 arcsec, and its variations are due to 274-d periodic Io-Europa quasiresonant interactions, and to 9.85-y precession of the orbital nodes. In this table and the previous one (6), we give all terms given by the frequency analysis.

The polar motion of the mantle (Fig.4 & Tab.8) is very small, the mean amplitude of 137.324 mas corresponding to 1.209 m in considering the polar radius  $c = 1,815.7$  km. For so small quantities, the digits given by the numerical frequency analysis lack of reliability, because they are very sensitive to the very small remaining amplitudes of the free librations. We show here terms whose amplitude is bigger than 20 milli-arcsec. The variations are

Table 6: Frequency analysis of the longitudinal librations  $\phi_m$ , in the Model 1. The series are in sine.

	Amplitude (arcsec)	Frequency (rad/y)	Phase (J2000.0)	Period (d)	Identification
1	−39.792	4.96186	−172.463	462.514	$\lambda_1^\bullet - 2\lambda_2^\bullet + \varpi_2^\bullet$
2	−30.731	1,301.919	60.879	1.76273	$2\lambda_1^\bullet - 2\lambda_2^\bullet$
3	−20.139	4.76032	−66.209	482.097	$\lambda_1^\bullet - 2\lambda_2^\bullet + \varpi_3^\bullet$
4	−17.601	1.11413	151.694	2,059.835	$\psi^\bullet$

Table 7: Frequency analysis of the obliquity of the mantle  $\epsilon_m$ , in the Model 1. The series are in cosine.

	Amplitude (arcsec)	Frequency (rad/y)	Phase (J2000.0)	Period (d)	Identification
1	7.88143	0	0	$\infty$	cst
2	2.35206	8.374973	−15.890	274.023	$2\lambda_1^\bullet - 4\lambda_2^\bullet + \Omega_1^\bullet + \Omega_2^\bullet$
3	0.50730	0.637684	−73.351	3,598.855	$\Omega_2^\bullet - \Omega_1^\bullet$
4	0.17966	16.74995	148.219	137.011	$3\lambda_1^\bullet - 5\lambda_2^\bullet - 2\lambda_3^\bullet + 2\Omega_1^\bullet + 2\Omega_2^\bullet$
5	0.07709	7.737289	−122.540	296.607	$\lambda_1^\bullet - \lambda_2^\bullet - 2\lambda_3^\bullet + 2\Omega_1^\bullet$
6	0.06353	1.904935	35.863	1,204.731	$2\lambda_{\odot}^\bullet - \Omega_1^\bullet - \Omega_{\odot}^\bullet$

dominated by two oscillations with short and close periods, that result in large variations over a wider timescale (Fig.4).

Finally, the tilt of the core can reach 9 arcsec, with the same kind of variations as the obliquity of the mantle  $\epsilon_m$ . In this last quasiperiodic decomposition (Tab.9), the cut-off is 0.1 arcsec.

We present on the Fig.5 the same outputs for the Model 2 (core made of FeS). The most striking difference involves the tilt of the velocity field of the fluid, oscillating between 5 and 25 arcsec. This tilt is bigger than the one of Model 1 (core of pure iron), this is due to the smaller value of  $\epsilon_3$  (Tab.3) that moves the system close to the resonance between the FCN  $\omega_z$  and the orbital frequency  $n$  (Tab.5) and raises the amplitude of the tilt, as already noticed in (Noyelles 2012).

The longitudinal librations are usually considered to be one of the easiest (or least difficult) rotational outputs to observe, particularly thanks to Earth-based radar observations, as did for instance Margot et al. (2007) for Mercury, detecting the its liquid core. That is the reason why we compare the longitudinal librations in the first two models, over 35 days (Fig.6).

Table 8: Frequency analysis of the amplitude of the polar motion of the mantle  $J_m$ , in the Model 1. The series are in cosine.

	Amplitude (mas)	Frequency (rad/y)	Phase (J2000.0)	Period (d)	Identification
1	137.324	0	0	$\infty$	cst
2	78.979	1,301.919	-29.121	1.76273	$2\lambda_1^\bullet - 2\lambda_2^\bullet$
3	71.518	1,294.181	-86.590	1.77327	$2\lambda_2^\bullet - 2\Omega_1^\bullet$
4	42.141	2,596.100	-115.715	0.88399	$2\lambda_1^\bullet - 2\Omega_1^\bullet$
5	36.616	8.374976	-15.918	274.023	$2\lambda_1^\bullet - 4\lambda_2^\bullet + \Omega_1^\bullet + \Omega_2^\bullet$
6	32.138	1,302.556	-102.458	1.76187	$2\lambda_1^\bullet - 2\lambda_2^\bullet + \Omega_2^\bullet - \Omega_1^\bullet$
7	22.167	2,604.475	-131.597	0.88115	$4\lambda_1^\bullet - 4\lambda_2^\bullet + \Omega_2^\bullet - \Omega_1^\bullet$

Table 9: Frequency analysis of the amplitude of the tilt of the fluid  $J_c$ , in the Model 1. The series are in cosine.

	Amplitude (arcsec)	Frequency (rad/y)	Phase (J2000.0)	Period (d)	Identification
1	5.89886	0	0	$\infty$	cst
2	2.69264	8.374973	-15.891	274.023	$2\lambda_1^\bullet - 4\lambda_2^\bullet + \Omega_1^\bullet + \Omega_2^\bullet$
3	0.33932	0.637686	-73.351	3,598.848	$\Omega_2^\bullet - \Omega_1^\bullet$
4	0.32639	16.74995	148.218	137.011	$3\lambda_1^\bullet - 5\lambda_2^\bullet - 2\lambda_3^\bullet + 2\Omega_1^\bullet + 2\Omega_2^\bullet$

This zoom on a short timescale allows to highlight the response to the short-period excitations. We can see that the amplitude associated is slightly bigger for the Model 2.

Finally, the Tab.10 gives the interesting amplitudes related to the rotational outputs in the different models. These amplitudes are respectively :

- 462-d and 1.76-d longitudinal librations
- mean value of the polar motion  $\langle J_m \rangle$ . As said above, these numbers are so small that they might lack of reliability.
- mean value of the tilt of the velocity field of the fluid  $\langle J_c \rangle$ .
- mean obliquity  $\langle \epsilon_m \rangle$  and the amplitude associated with the 274-d sinusoidal excitation.

As before, we can see two groups: the "odd" models in which the core of Io is made of pure iron, and the "even" ones, in which the core is made of FeS. The impact on the

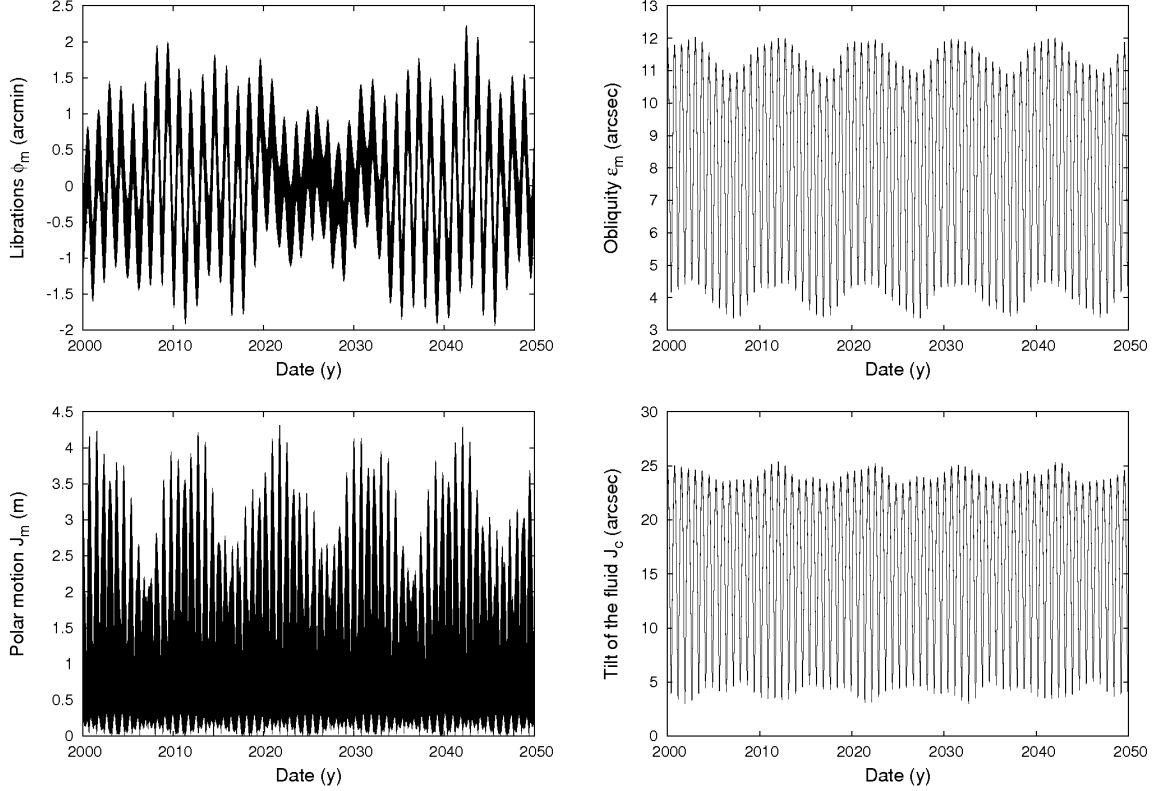


Fig. 5.— Observable outputs of the Model 2 (core made of FeS).

longitudinal librations is not so significant. In fact, we can check the numbers thanks to analytical formulae given e.g. in (Rambaux et al. 2010):

$$\phi = A_u \sin(\omega_u t + \phi_u) + \sum_i \frac{\omega_u^2 H_i}{\omega_u^2 - \omega_i^2} \sin(\omega_i t + \alpha_i), \quad (36)$$

where  $A_u$  and  $\phi_u$  and the amplitudes and phases associated with the free librations,  $A_u$  being here assumed to be very small,  $\omega_i$  are the forcing frequencies, in our case related to the proper modes given in the orbital ephemerides Tab.4, and  $H_i$  and  $\alpha_i$  are the amplitudes and phases associated in the expression of Io’s true orbital anomaly. Denoting  $\omega_1 = 4.96186$  rad/y and  $\omega_2 = 1,301.909$  rad/y, respectively associated with the periods  $T_1 = 462.514$  and  $T_2 = 1.76273$  days,  $A_1$  and  $A_2$  being the amplitudes associated in  $\phi_m$ , we have

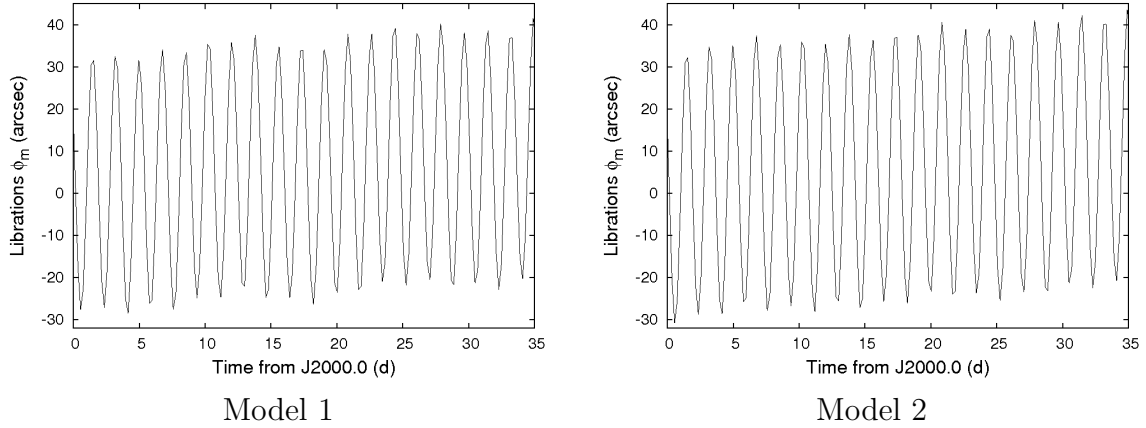


Fig. 6.— Expected longitudinal librations.

$$A_1 \propto \left| \frac{\omega_u^2}{\omega_u^2 - \omega_1^2} \right|, \quad (37)$$

$$A_2 \propto \left| \frac{\omega_u^2}{\omega_u^2 - \omega_2^2} \right|, \quad (38)$$

yielding a relative variation of  $\approx 5\%$  for  $A_1$  between the models 1 and 2, and of  $0.004\%$  for  $A_2$ . This is consistent with the numbers given in Tab.10.

The obliquity  $\epsilon_m$  is small, but its variations between the two groups of models are significant. In particular, the amplitude associated with the 274-d oscillation can be enhanced by 50% when the core is made of FeS. The most significant impact is on the mean amplitude of the tilt of the fluid  $\langle J_c \rangle$ , that can unfortunately not be directly measured. Finally, the impact of a differentiated rigid crust is very limited on the rotation outputs.

## 5. Elliptical instability

In all the calculations, we have assumed that the flow of the fluid is laminar. In fact, as initially seen experimentally by Pierrehumbert (1986) and theoretically explained by Bayly (1986) in the context of an unbounced strained uniform vortex, the periodic forcing of the elliptical cavity on the underlying rotation state produces a pairwise resonance of inertial waves which can grow exponentially. This studies follow independent predictions in the 1970s, the reader can find a review in (Kerswell 2002). To check the stability of the flow we need to consider the growth rate  $\sigma$  for an arbitrary perturbation  $\vec{v}$ , see e.g. (Kerswell & Malkus 1998):

Table 10: Variations of the outputs in the different models.

Models	$\phi_m$ (462 d) (arcsec)	$\phi_m$ (1.76 d) (arcsec)	$\langle J_m \rangle$ (mas)	$\langle J_c \rangle$ (arcsec)	$\langle \epsilon_m \rangle$ (arcsec)	$\epsilon_m$ (274 d) (arcsec)
1	39.82462	30.73077	136.592	5.89884	7.88443	2.35306
3	39.82475	30.60912	135.689	5.52936	7.87640	2.33113
5	39.82471	30.60990	140.266	4.71025	7.87421	2.32106
7	39.82475	30.58332	138.148	5.41307	7.87537	2.32659
9	39.82470	30.58433	140.037	4.43989	7.87308	2.31578
2	39.82303	32.35491	139.912	15.82812	8.14896	3.60967
4	39.82346	31.89343	140.550	13.13468	8.06166	3.08910
6	39.82343	31.89475	136.787	10.18116	7.99303	2.84826
8	39.82345	31.88809	136.018	12.78276	8.04716	3.07908
10	39.82342	31.88951	138.648	10.07450	7.99055	2.83580

$$\sigma(t) = \frac{1}{2} \frac{d \ln \langle \vec{v}^2 / 2 \rangle}{dt} = - \frac{\langle \vec{v} \cdot \vec{\nabla} U \cdot \vec{v} \rangle}{\langle \vec{v}^2 \rangle}, \quad (39)$$

where the flow  $\vec{U}$  is the velocity field of the fluid a priori assumed to be laminar (Eq.A3 to A5), and  $\langle \rangle = \int dV$ ,  $V$  being the volume of the fluid. The flow is stable when  $\sigma < 0$ , and unstable otherwise. Cebon et al. (2012) have recently derived the following formula:

$$\sigma(t) = n \left( \frac{(2\Omega^G(t) + 3)^2}{16 |1 + \Omega^G(t)|^3} \beta - 2.62 \frac{1 + \eta^4}{1 - \eta^5} \sqrt{E} - \frac{\Lambda}{4 |1 + \Omega^G(t)|^3} \right), \quad (40)$$

in the context of a triaxial body perturbed by a primary whose rotation axis is close to the geometrical polar axis, and is under the influence of a magnetic field. The parameters involved in this formula are:

- $\Omega^G(t) = \frac{n}{\Omega^s(t) - n} \approx \frac{1}{P(t) - 1}$  where  $\Omega^s$  is the spin frequency of Io ((Cebon et al. 2012) assumed it to be collinear to the geometrical polar axis)
- $\beta = \frac{a_s^2 - b_s^2}{a_s^2 + b_s^2}$
- $\eta$ : ratio between the internal and the external radii of the fluid layer. Equal to 0 for fully liquid core.
- Ekman number  $E = \frac{\nu}{\Omega R_c^2}$  where  $\nu$  is the fluid kinematic viscosity, and  $\Omega = n P_c / \delta = n$  the mean velocity of the fluid. This is a kind of adimensional viscosity.

- Elsasser number  $\Lambda = \frac{\sigma_e B_0^2}{\rho_c \Omega}$ , where  $B_0$  is the intensity of the magnetic field and  $\sigma_e$  the fluid electrical conductivity. This contribution of the magnetic field has been derived by Herreman et al. (2009).

As Herreman et al. (2009); Cebon et al. (2012) did, we took  $B_0 = 1850nT$ ,  $\nu = 10^{-6}m^2s^{-1}$  and  $\sigma_e = 4 \times 10^5 S.m^{-1}$ . This yields the numbers given in Tab.11.

Table 11: Parameters used to compute the grow rate  $\sigma$ .

Models	$\beta$	$\eta$	$E$	$\Lambda$
1	$4.419 \times 10^{-2}$	0	$5.389 \times 10^{-14}$	$4.163 \times 10^{-6}$
3	$5.345 \times 10^{-2}$	0	$6.026 \times 10^{-14}$	$4.163 \times 10^{-6}$
5	$5.673 \times 10^{-2}$	0	$6.026 \times 10^{-14}$	$4.163 \times 10^{-6}$
7	$5.638 \times 10^{-2}$	0	$6.150 \times 10^{-14}$	$4.163 \times 10^{-6}$
9	$6.060 \times 10^{-2}$	0	$6.150 \times 10^{-14}$	$4.163 \times 10^{-6}$
2	$2.114 \times 10^{-2}$	0	$2.612 \times 10^{-14}$	$6.467 \times 10^{-6}$
4	$2.487 \times 10^{-2}$	0	$2.859 \times 10^{-14}$	$6.467 \times 10^{-6}$
6	$2.616 \times 10^{-2}$	0	$2.859 \times 10^{-14}$	$6.467 \times 10^{-6}$
8	$2.505 \times 10^{-2}$	0	$2.862 \times 10^{-14}$	$6.467 \times 10^{-6}$
10	$2.638 \times 10^{-2}$	0	$2.862 \times 10^{-14}$	$6.467 \times 10^{-6}$

The instantaneous growth rate for the Model 1 is plotted in Fig.7.

We can see that  $\sigma$  exhibits oscillations coming from  $P(t)$ , that make its sign vary. To check the stability of the inertial waves, we need to average  $\sigma$ . The results are given in Tab.12.

The mean growth rate  $\langle \sigma \rangle$  is positive in every model. Anyway, it is smaller in the "even" models, i.e. with a FeS core, with a growth time of the order of 5,000 years (twice bigger if we neglect the crust in Model 2), while it is always smaller than 2,000 years in the "odd" models (Fe core). For comparison we give in the last column the spin-up time  $t_{spin-up} = 1/(n\sqrt{E})$  (Greenspan & Howard 1963). This is the typical spin-up/spin-down time necessary for the fluid to recover the mantle velocity.  $t_{spin-up}$  is usually assumed to be long enough so that the velocity of the fluid can be considered as constant. It is actually long with respect to the periods of the oscillations of the gravitational torque of Jupiter (see Tab.4, the longer period being  $\approx 560$  years). However, we can notice that this time is of the order of magnitude of the growth time  $1/\langle \sigma \rangle$ .

In all these models we find that the inertial waves of the core of Io should be unstable. It is in fact assumed since (Kerswell & Malkus 1998) that they are unstable, this has been

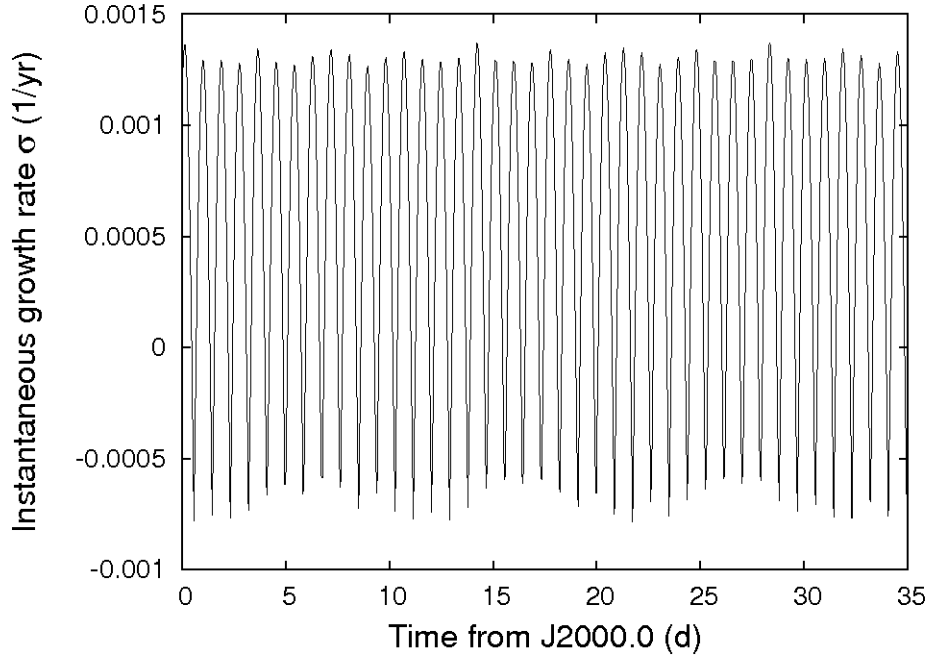


Fig. 7.— Growth rate in the model 1.

confirmed by (Herreman et al. 2009) in adding the influence of the magnetic field. This last reference suggests a growth time of  $\approx 63$  years. However, (Cebon et al. 2012) argue that this growth rate has been calculated in an extreme optimal case, in particular in considering an extremum of the instantaneous departure from the synchronous rotation. They conclude that the inertial waves in Io’s fluid core should be stable. Our result lies between these two opposite conclusions, i.e. a positive but quite small growth rate. The main difference between our study and the previous ones is that we consider instantaneous variations of the velocity of the mantle, computed from a complete model. Another difference comes from the ellipticity of the core  $\beta$ , assumed to be 0.006 in the previous studies, and derived from our 10 models in this study. We get this way bigger ellipticities (Tab.11), that favour the elliptical instability.

We finally propose to estimate the different contributions in the elliptical instability. For that we rewrite the formula (40) as

$$\sigma(t) = \sigma_1(t) + \sigma_2 + \sigma_3(t) \quad (41)$$

with

Table 12: Mean grow rate  $\langle \sigma \rangle$ , and the time associated compared with the spin-up time  $t_{spin-up}$ .

Models	$\langle \sigma \rangle$ ( $yr^{-1}$ )	$1/\langle \sigma \rangle$ ( $kyr$ )	$t_{spin-up}$ ( $kyr$ )
1	$5.528 \times 10^{-4}$	1.809	3.321
3	$7.885 \times 10^{-4}$	1.268	3.140
5	$8.881 \times 10^{-4}$	1.126	3.140
7	$8.689 \times 10^{-4}$	1.151	3.109
9	$9.971 \times 10^{-4}$	1.003	3.109
2	$9.320 \times 10^{-5}$	10.729	4.770
4	$1.810 \times 10^{-4}$	5.525	4.559
6	$2.202 \times 10^{-4}$	4.541	4.559
8	$1.861 \times 10^{-4}$	5.373	4.557
10	$2.266 \times 10^{-4}$	4.413	4.557

$$\sigma_1(t) = n \frac{(2\Omega^G(t) + 3)^2}{16 |1 + \Omega^G(t)|^3} \beta, \quad (42)$$

$$\sigma_2 = -2.62n \frac{1 + \eta^4}{1 - \eta^5} \sqrt{E}, \quad (43)$$

$$\sigma_3(t) = -\frac{n\Lambda}{4 |1 + \Omega^G(t)|^3}. \quad (44)$$

We get for the Model 1:

- $\langle \sigma \rangle = 5.528 \times 10^{-4} yr^{-1}$ ,
- $\langle \sigma_1 \rangle = 1.342 \times 10^{-3} yr^{-1}$ ,
- $\sigma_2 = -7.890 \times 10^{-4} yr^{-1}$ ,
- $\langle \sigma_3 \rangle = -1.824 \times 10^{-15} yr^{-1}$ .

We see that the influence of the magnetic field ( $\sigma_3$ ) is negligible with respect to the other contributions. In fact, the stability (or unstability) is a consequence of a balance between  $\sigma_1$  and  $\sigma_2$ .

## 6. Conclusion

This paper consists of 3 parts: an elaboration of 10 interior models of Io based on the measured  $J_2$  and  $C_{22}$ , a computation of its rotation in considering pressure coupling at the core-mantle boundary, and a discussion on the elliptical instability inside the core. We have seen that the most significant assumption involves the composition of the core, i.e. either pure iron (Fe) or a eutectic mixture of iron and sulfur (FeS).

In both cases, the amplitude of the short longitudinal librations is about 30 arcsec, and the mean obliquity  $\approx 8$  arcsec, these two quantities being a little bigger for a FeS core, which is larger. But the main difference is in the tilt of the angular momentum of the fluid constituting the core, that is bigger (between 10 and 15 arcsec) for the FeS than for the Fe one ( $\approx 5$  arcsec). A study of the elliptical instability indicates that the inertial waves should be unstable in any case, the growth time being between 1 and 2 kyr for a Fe core and between 5 and 10 kyr for a FeS core. This last calculation only considers the influence of the longitudinal librations, without involving the tilt of the fluid.

Using the measured value of the gravity coefficients  $J_2$  and  $C_{22}$  leads to a triaxial core whose polar axis is not the smallest one, that is somehow counterintuitive for a body in hydrostatic equilibrium. We hope that future space missions will allow to collect more data on Io's dynamics and internal structure. Unfortunately, Io is currently the target of no space mission, the ESA proposal JUICE being focused on Europa and Ganymede.

## Acknowledgements

This research used resources of the Interuniversity Scientific Computing Facility located at the University of Namur, Belgium, which is supported by the F.R.S.-FNRS under convention No. 2.4617.07. The author is F.R.S.-FNRS post-doctoral research fellow.

### A. Hamiltonian formulation of the Poincaré-Hough model

In this reference frame  $(\vec{f}_1, \vec{f}_2, \vec{f}_3)$  bound to the principal axes of inertia of Io, the matrix of inertia reads:

$$I = \begin{pmatrix} A & 0 & 0 \\ 0 & B & 0 \\ 0 & 0 & C \end{pmatrix} \quad (\text{A1})$$

with  $0 < A \leq B \leq C$ , while that of the core is:

$$I_c = \begin{pmatrix} A_c & 0 & 0 \\ 0 & B_c & 0 \\ 0 & 0 & C_c \end{pmatrix}, \quad (\text{A2})$$

in the same reference frame. So, the orientations of the mantle and the cavity are the same.

In this way, the principal moments of inertia of the mantle are respectively  $A_m = A - A_c$ ,  $B_m = B - B_c$  and  $C_m = C - C_c$ . The principal elliptical radii of the cavity are written respectively  $a, b, c$ , yielding

$$\begin{aligned} A_c &= \iiint (x_2^2 + x_3^2) \rho \, dx_1 \, dx_2 \, dx_3 = \frac{M_c}{5} (b^2 + c^2), \\ B_c &= \iiint (x_1^2 + x_3^2) \rho \, dx_1 \, dx_2 \, dx_3 = \frac{M_c}{5} (a^2 + c^2), \\ C_c &= \iiint (x_1^2 + x_2^2) \rho \, dx_1 \, dx_2 \, dx_3 = \frac{M_c}{5} (a^2 + b^2), \end{aligned}$$

where  $\rho$  and  $M_c$  are respectively the mass density and the mass of the fluid core, the quadrature being performed over the volume of the core.

#### A.1. The kinetic energy of the system

A Hamiltonian formulation of such a problem is usually composed of a kinetic energy and a disturbing potential, here the perturbation of the planet. Therefore, we consider every internal process, as the core-mantle interactions in our case, as part of the kinetic energy of the satellite. This section is widely inspired from (Henrard 2008).

The components  $(v_1, v_2, v_3)$  of the velocity field at the location  $(x_1, x_2, x_3)$  inside the liquid core, in the frame of the principal axes of inertia of the mantle, are assumed to be (Poincaré 1910):

$$v_1 = \left( \omega_2 + \frac{a}{c} \nu_2 \right) x_3 - \left( \omega_3 + \frac{a}{b} \nu_3 \right) x_2, \quad (\text{A3})$$

$$v_2 = \left( \omega_3 + \frac{b}{a} \nu_3 \right) x_1 - \left( \omega_1 + \frac{b}{c} \nu_1 \right) x_3, \quad (\text{A4})$$

$$v_3 = \left( \omega_1 + \frac{c}{b} \nu_1 \right) x_2 - \left( \omega_2 + \frac{c}{a} \nu_2 \right) x_1, \quad (\text{A5})$$

where  $(\omega_1, \omega_2, \omega_3)$  are the components of the angular velocity of the mantle with respect to an inertial frame, and the vector of coordinates  $(\nu_1, \nu_2, \nu_3)$  specifies the velocity field of the core with respect to the moving mantle. Here we assume that this velocity field  $(\nu_1, \nu_2, \nu_3)$  depends only on the time  $t$ , and not on the spatial coordinates  $(x_1, x_2, x_3)$ . It implies that we have

$$\vec{\nabla} \cdot \vec{v} = \frac{\partial v_1}{\partial x_1} + \frac{\partial v_2}{\partial x_2} + \frac{\partial v_3}{\partial x_3} = 0, \quad (\text{A6})$$

this equation is known as the continuity equation.

The angular momentum of the core  $\vec{N}'_c$  is obtained by:

$$\vec{N}'_c = \iiint_{\text{core}} (\vec{x} \times \vec{v}) \rho \, dx_1 \, dx_2 \, dx_3 \quad (\text{A7})$$

and the result is:

$$\begin{aligned} \vec{N}'_c = & \frac{M_c}{5} \left[ \left( \frac{c}{b} \nu_1 + \omega_1 \right) b^2 + \left( \frac{b}{c} \nu_1 + \omega_1 \right) c^2 \right] \vec{f}_1 \\ & + \frac{M_c}{5} \left[ \left( \frac{c}{a} \nu_2 + \omega_2 \right) a^2 + \left( \frac{a}{c} \nu_2 + \omega_2 \right) c^2 \right] \vec{f}_2 \\ & + \frac{M_c}{5} \left[ \left( \frac{b}{a} \nu_3 + \omega_3 \right) a^2 + \left( \frac{a}{b} \nu_3 + \omega_3 \right) b^2 \right] \vec{f}_3. \end{aligned} \quad (\text{A8})$$

We now set the following quantities:

$$\begin{aligned} D_1 &= \frac{2M_c}{5} bc = \sqrt{(A_c - B_c + C_c)(A_c + B_c - C_c)}, \\ D_2 &= \frac{2M_c}{5} ac = \sqrt{(-A_c + B_c + C_c)(A_c + B_c - C_c)}, \\ D_3 &= \frac{2M_c}{5} ab = \sqrt{(-A_c + B_c + C_c)(A_c - B_c + C_c)}, \end{aligned}$$

that have the dimension of moments of inertia and can be seen as parameters of the core as  $A_c$ ,  $B_c$  and  $C_c$ , and we can write:

$$\vec{N}'_c = [A_c\omega_1 + D_1\nu_1]\vec{f}_1 + [B_c\omega_2 + D_2\nu_2]\vec{f}_2 + [C_c\omega_3 + D_3\nu_3]\vec{f}_3, \quad (\text{A9})$$

while the angular momentum of the mantle is

$$\vec{N}_m = A_m\omega_1\vec{f}_1 + B_m\omega_2\vec{f}_2 + C_m\omega_3\vec{f}_3, \quad (\text{A10})$$

and the total angular momentum of Io is

$$\vec{N} = [A\omega_1 + D_1\nu_1]\vec{f}_1 + [B\omega_2 + D_2\nu_2]\vec{f}_2 + [C\omega_3 + D_3\nu_3]\vec{f}_3. \quad (\text{A11})$$

The kinetic energy of the core is

$$T_c = \frac{1}{2} \iiint_{core} \rho v^2 dx_1 dx_2 dx_3 \quad (\text{A12})$$

i.e.

$$T_c = \frac{1}{2} \left( A_c(\omega_1^2 + \nu_1^2) + B_c(\omega_2^2 + \nu_2^2) + C_c(\omega_3^2 + \nu_3^2) + 2D_1\omega_1\nu_1 + 2D_2\omega_2\nu_2 + 2D_3\omega_3\nu_3 \right), \quad (\text{A13})$$

while the kinetic energy of the mantle  $T_m$  is

$$T_m = \frac{1}{2} \vec{N}_m \cdot \vec{\omega} = \frac{A_m\omega_1^2 + B_m\omega_2^2 + C_m\omega_3^2}{2}. \quad (\text{A14})$$

From  $T = T_m + T_c$  we finally deduce the kinetic energy of the satellite:

$$T = \frac{1}{2} \left( A\omega_1^2 + B\omega_2^2 + C\omega_3^2 + A_c\nu_1^2 + B_c\nu_2^2 + C_c\nu_3^2 + 2D_1\omega_1\nu_1 + 2D_2\omega_2\nu_2 + 2D_3\omega_3\nu_3 \right). \quad (\text{A15})$$

We can easily check the expressions of the partial derivatives, for instance

$$\frac{\partial T}{\partial \omega_1} = A\omega_1 + D_1\nu_1 = N_1 \quad (\text{A16})$$

or

$$\frac{\partial T}{\partial \nu_1} = D_1 \omega_1 + A_c \nu_1 = N_1^c, \quad (\text{A17})$$

where  $N_i$  are the components of the total angular momentum.  $N_i^c$  are not the components of the angular momentum of the core but are close to it for a cavity close to spherical. We have, for instance for the first component:

$$N_1^c - N_1'^c = (A_c - D_1)(\omega_1 - \nu_1) = \frac{M_c}{5}(c - b)^2(\omega_1 - \nu_1), \quad (\text{A18})$$

so the difference is of the second order in departure from the sphericity. From now on, we call *angular momentum of the pseudo-core* the vector  $\vec{N}^c = N_1^c \vec{f}_1 + N_2^c \vec{f}_2 + N_3^c \vec{f}_3$ .

With these notations, the Poincaré-Hough's equations of motion, for the system mantle-core in the absence of external torque, are (see e.g. Eq.15 in Touma & Wisdom (2001) or Henrard (2008)):

$$\frac{d\vec{N}}{dt} = \vec{N} \times \vec{\nabla}_{\vec{N}} \mathcal{T}, \quad (\text{A19})$$

$$\frac{d\vec{N}^c}{dt} = \vec{N}^c \times \vec{\nabla}_{-\vec{N}^c} \mathcal{T}, \quad (\text{A20})$$

with

$$\vec{\nabla}_{\vec{N}} \mathcal{T} = \frac{\partial \mathcal{T}}{\partial N_1} \vec{f}_1 + \frac{\partial \mathcal{T}}{\partial N_2} \vec{f}_2 + \frac{\partial \mathcal{T}}{\partial N_3} \vec{f}_3, \quad (\text{A21})$$

and

$$\vec{\nabla}_{-\vec{N}^c} \mathcal{T} = -\frac{\partial \mathcal{T}}{\partial N_1^c} \vec{f}_1 - \frac{\partial \mathcal{T}}{\partial N_2^c} \vec{f}_2 - \frac{\partial \mathcal{T}}{\partial N_3^c} \vec{f}_3. \quad (\text{A22})$$

Here  $\mathcal{T}$  is the kinetic energy expressed in terms of the components of the vectors  $\vec{N}$  and  $\vec{N}^c$ , i.e.

$$\begin{aligned} \mathcal{T} = \frac{1}{2\alpha} (A_c N_1^2 + A(N_1^c)^2 - 2D_1 N_1 N_1^c) &+ \frac{1}{2\beta} (B_c N_2^2 + B(N_2^c)^2 - 2D_2 N_2 N_2^c) \\ &+ \frac{1}{2\gamma} (C_c N_3^2 + C(N_3^c)^2 - 2D_3 N_3 N_3^c) \end{aligned} \quad (\text{A23})$$

with  $\alpha = AA_c - D_1^2$ ,  $\beta = BB_c - D_2^2$  and  $\gamma = CC_c - D_3^2$ .

## A.2. The Hamiltonian

### A.2.1. The rotational kinetic energy

We assume that the cavity and the satellite are almost spherical, this allows us to introduce the four small parameters  $\epsilon_i$ :

$$\epsilon_1 = \frac{2C - A - B}{2C} = J_2 \frac{MR^2}{C}, \quad (\text{A24})$$

$$\epsilon_2 = \frac{B - A}{2C} = 2C_{22} \frac{MR^2}{C}, \quad (\text{A25})$$

$$\epsilon_3 = \frac{2C_c - A_c - B_c}{2C_c}, \quad (\text{A26})$$

$$\epsilon_4 = \frac{B_c - A_c}{2C_c}, \quad (\text{A27})$$

where  $M$  is the mass of our body and  $R$  its mean radius, and also the parameter  $\delta = C_c/C$ , i.e. the ratio between the polar inertial momentum of the core and of the satellite.  $\epsilon_1$  represents the polar flattening of the satellite, while  $\epsilon_2$  is its equatorial ellipticity.  $\epsilon_3$  and  $\epsilon_4$  have the same meaning for the cavity.

We now introduce the two sets of Andoyer's variables (Andoyer 1926),  $(l, g, h, L, G, H)$  and  $(l_c, g_c, h_c, L_c, G_c, H_c)$ , related respectively to the whole satellite and to its core. The angles  $(h, K, g)$  are the Euler angles of the vector  $\vec{n}_2$ , node of the equatorial plane over the plane perpendicular to the angular momentum  $\vec{N}$ , the angles  $(J, l)$  position the axis of least inertia  $\vec{f}_1$  with respect to  $\vec{n}_2$ . Correspondingly the angles  $(h_c, K_c, g_c)$  are the Euler angles of the vector  $\vec{n}_2^c$ , node of the equatorial plane over the plane perpendicular to the angular momentum of the pseudo-core  $\vec{N}^c$ , and  $(J_c, l_c)$  position the axis of least inertia with respect to  $\vec{n}_2^c$ . The Figure 3 shows a schematic view of all the reference frames and relevant angles. The variables are  $(h, g, l)$  and  $(h_c, g_c, l_c)$  and the corresponding momenta ( $H = N \cos K$ ,  $G = N$ ,  $L = N \cos J$ ) and ( $H_c = N^c \cos K_c$ ,  $G_c = N^c$ ,  $L_c = N^c \cos J_c$ ). Expressed in Andoyer's variables the components of  $\vec{N}$  and  $\vec{N}^c$  are:

$$\begin{aligned} N_1 &= \sqrt{G^2 - L^2} \sin l, & N_1^c &= \sqrt{G_c^2 - L_c^2} \sin l_c, \\ N_2 &= \sqrt{G^2 - L^2} \cos l, & N_2^c &= \sqrt{G_c^2 - L_c^2} \cos l_c, \\ N_3 &= L, & N_3^c &= L_c. \end{aligned}$$

We can now straightforwardly derive the Hamiltonian  $\mathcal{H}_1$  of the free rotation of the satellite, using Andoyer's variables and changing the sign of  $\vec{N}^c$  to take the minus sign of the

Poincaré-Hough equations into account (Eq.A20). We also linearize the Hamiltonian with respect to the small parameters  $\epsilon_i$  (their orders of magnitude being about  $10^{-2}$ , see Tab.3), and get:

$$\begin{aligned}
\mathcal{H}_0 = & \frac{1}{2C(1-\delta)} \left( G^2 + \frac{G_c^2}{\delta} + 2\sqrt{(G^2 - L^2)(G_c^2 - L_c^2)} \cos(l - l_c) + 2LL_c \right) \\
& + \frac{\epsilon_1}{2C(1-\delta)^2} \left( G^2 - L^2 + G_c^2 - L_c^2 + 2\sqrt{(G^2 - L^2)(G_c^2 - L_c^2)} \cos(l - l_c) \right) \\
& - \frac{\epsilon_2}{2C(1-\delta)^2} \left( (G^2 - L^2) \cos(2l) + (G_c^2 - L_c^2) \cos(2l_c) \right. \\
& \quad \left. + 2\sqrt{(G^2 - L^2)(G_c^2 - L_c^2)} \cos(l + l_c) \right) \\
& - \frac{\epsilon_3}{2C(1-\delta)^2} \left( \delta(G^2 - L^2) + (G_c^2 - L_c^2)(2 - \frac{1}{\delta}) \right. \\
& \quad \left. + 2\delta\sqrt{(G^2 - L^2)(G_c^2 - L_c^2)} \cos(l - l_c) \right) \\
& + \frac{\epsilon_4}{2C(1-\delta)^2} \left( \delta(G^2 - L^2) \cos(2l) + (G_c^2 - L_c^2)(2 - \frac{1}{\delta}) \cos(2l_c) \right. \\
& \quad \left. + 2\delta\sqrt{(G^2 - L^2)(G_c^2 - L_c^2)} \cos(l + l_c) \right). \tag{A28}
\end{aligned}$$

We now introduce the following canonical change of variables, of multiplier  $\frac{1}{nC}$ ,  $n$  being the mean orbital motion of the satellite:

$$\begin{aligned}
p &= l + g + h, & P &= \frac{G}{nC}, \\
r &= -h, & R &= P(1 - \cos K), \\
\xi_1 &= -\sqrt{2P(1 - \cos J)} \sin l, & \eta_1 &= \sqrt{2P(1 - \cos J)} \cos l, \\
p_c &= -l_c + g_c + h_c, & P_c &= \frac{G_c}{nC}, \\
r_c &= -h_c, & R_c &= P_c(1 - \cos K_c), \\
\xi_2 &= \sqrt{2P_c(1 + \cos J_c)} \sin l_c, & \eta_2 &= \sqrt{2P_c(1 + \cos J_c)} \cos l_c.
\end{aligned} \tag{A29}$$

The first three lines of this new set of variables and associated moments are related to the whole body, while the last three ones are related to the pseudo-core.  $P$  is the normalized norm of the angular momentum, it should be close to 1 at the spin-orbit resonance. Since the obliquity  $K$  is small, we have  $R \propto K^2$ , i.e. this is a small quantity related to the obliquity of the body. The quantities  $(\xi_1, \eta_1)$  are related to the polar motion of the whole Io, i.e. the angle

$J$  between the geometrical polar axis and the angular momentum, while  $l$  is the precession angle associated. We can note that  $\xi_1$  and  $\eta_1$  are always defined, while  $l$  is not defined when  $J = 0$ . The last three lines have basically the same meaning for the pseudo-core. We will see later that the degree of freedom  $(r_c, R_c)$  is in fact not involved in the dynamics of this model, and that  $p_c$  is not involved either, letting the norm of the angular momentum of the pseudo-core  $P_c$  be a constant. So, we can consider that the rotational dynamics of our body has 4, and not 6, degrees of freedom.

In order to be consistent with the minus sign in the equations and before  $l_c$ , the amplitude of the wobble of the pseudo-core  $J_c$  has to be replaced by  $\pi - J_c$ . In this way, we have  $L_c = G_c \cos(\pi - J_c) = -G_c \cos(J_c)$ . In this new set of variables, we have

$$\begin{aligned} N_1 &= -nC \sqrt{P^2 - \left(P - \frac{\xi_1^2 + \eta_1^2}{2}\right)^2} \frac{\xi_1}{\xi_1^2 + \eta_1^2}, & N_1^c &= nC \sqrt{P_c^2 - \left(\frac{\xi_2^2 + \eta_2^2}{2} - P_c\right)^2} \frac{\xi_2}{\xi_2^2 + \eta_2^2}, \\ N_2 &= nC \sqrt{P^2 - \left(P - \frac{\xi_1^2 + \eta_1^2}{2}\right)^2} \frac{\eta_1}{\xi_1^2 + \eta_1^2}, & N_2^c &= nC \sqrt{P_c^2 - \left(\frac{\xi_2^2 + \eta_2^2}{2} - P_c\right)^2} \frac{\eta_2}{\xi_2^2 + \eta_2^2}, \\ N_3 &= nC \left(P - \frac{\xi_1^2 + \eta_1^2}{2}\right), & N_3^c &= nC \left(\frac{\xi_2^2 + \eta_2^2}{2} - P_c\right), \end{aligned}$$

and the Hamiltonian of the free rotational motion becomes, after division by  $nC$ :

$$\begin{aligned}
\mathcal{H}_1 = & \frac{n}{2(1-\delta)} \left( P^2 + \frac{P_c^2}{\delta} + 2\sqrt{\left(P - \frac{\xi_1^2 + \eta_1^2}{4}\right)\left(P_c - \frac{\xi_2^2 + \eta_2^2}{4}\right)} (\eta_1\eta_2 - \xi_1\xi_2) \right. \\
& \left. + 2\left(P - \frac{\xi_1^2 + \eta_1^2}{2}\right)\left(\frac{\xi_2^2 + \eta_2^2}{2} - P_c\right) \right) \\
& + \frac{n\epsilon_1}{2(1-\delta)^2} \left( P_c^2 - \left(\frac{\xi_2^2 + \eta_2^2}{2} - P_c\right)^2 + P^2 - \left(P - \frac{\xi_1^2 + \eta_1^2}{2}\right)^2 \right. \\
& \left. + 2\sqrt{\left(P - \frac{\xi_1^2 + \eta_1^2}{4}\right)\left(P_c - \frac{\xi_2^2 + \eta_2^2}{4}\right)} (\eta_1\eta_2 - \xi_1\xi_2) \right) \\
& + \frac{n\epsilon_2}{2(1-\delta)^2} \left( \frac{1}{4}(4P - \xi_1^2 - \eta_1^2)(\xi_1^2 - \eta_1^2) + \frac{1}{4}(4P_c - \xi_2^2 - \eta_2^2)(\xi_2^2 - \eta_2^2) \right. \\
& \left. - 2\sqrt{\left(P - \frac{\xi_1^2 + \eta_1^2}{4}\right)\left(P_c - \frac{\xi_2^2 + \eta_2^2}{4}\right)} (\eta_1\eta_2 + \xi_1\xi_2) \right) \\
& - \frac{n\epsilon_3}{2(1-\delta)^2} \left( \delta\left(P^2 - \left(P - \frac{\xi_1^2 + \eta_1^2}{2}\right)^2\right) + \left(P_c^2 - \left(\frac{\xi_2^2 + \eta_2^2}{2} - P_c\right)^2\right)\left(2 - \frac{1}{\delta}\right) \right. \\
& \left. + 2\delta\sqrt{\left(P - \frac{\xi_1^2 + \eta_1^2}{4}\right)\left(P_c - \frac{\xi_2^2 + \eta_2^2}{4}\right)} (\eta_1\eta_2 - \xi_1\xi_2) \right) \\
& + \frac{n\epsilon_4}{2(1-\delta)^2} \left( \frac{\delta}{4}(4P - \xi_1^2 - \eta_1^2)(\eta_1^2 - \xi_1^2) + \left(2 - \frac{1}{\delta}\right)\frac{1}{4}(4P_c - \xi_2^2 - \eta_2^2)(\eta_2^2 - \xi_2^2) \right. \\
& \left. + 2\delta\sqrt{\left(P - \frac{\xi_1^2 + \eta_1^2}{4}\right)\left(P_c - \frac{\xi_2^2 + \eta_2^2}{4}\right)} (\eta_1\eta_2 + \xi_1\xi_2) \right). \tag{A30}
\end{aligned}$$

Finally, in order to get an easy-to-read formula, we can develop this Hamiltonian up to the second order in  $(\xi_1, \xi_2, \eta_1, \eta_2)$  to get:

$$\begin{aligned}
\mathcal{H}_1 \approx & \frac{n}{2(1-\delta)} \left( P^2 + \frac{P_c^2}{\delta} + 2\sqrt{PP_c}(\eta_1\eta_2 - \xi_1\xi_2) \right. \\
& \left. + 2\left( P\frac{\xi_2^2 + \eta_2^2}{2} + P_c\frac{\xi_1^2 + \eta_1^2}{2} - PP_c \right) \right) \\
& + \frac{n\epsilon_1}{2(1-\delta)^2} \left( P(\xi_1^2 + \eta_1^2) + P_c(\xi_2^2 + \eta_2^2) + 2\sqrt{PP_c}(\eta_1\eta_2 - \xi_1\xi_2) \right) \\
& + \frac{n\epsilon_2}{2(1-\delta)^2} \left( P(\xi_1^2 - \eta_1^2) + P_c(\xi_2^2 - \eta_2^2) - 2\sqrt{PP_c}(\eta_1\eta_2 + \xi_1\xi_2) \right) \\
& - \frac{n\epsilon_3}{2(1-\delta)^2} \left( \delta P(\xi_1^2 + \eta_1^2) + \left(2 - \frac{1}{\delta}\right) P_c(\xi_2^2 + \eta_2^2) + 2\delta\sqrt{PP_c}(\eta_1\eta_2 - \xi_1\xi_2) \right) \\
& + \frac{n\epsilon_4}{2(1-\delta)^2} \left( \delta P(\eta_1^2 - \xi_1^2) + \left(2 - \frac{1}{\delta}\right) P_c(\eta_2^2 - \xi_2^2) + 2\delta\sqrt{PP_c}(\eta_1\eta_2 + \xi_1\xi_2) \right).
\end{aligned} \tag{A31}$$

This is in fact a third-order development since the powers in  $(\xi_1, \xi_2, \eta_1, \eta_2)$  are even. In all the computations presented in this paper, this last approximation has not been used, the equations we have propagated deriving from the Hamiltonian (A30), same as (27).

### A.2.2. The gravitational potential

To compute the gravitational potential due to Jupiter on Io, we must first obtain the coordinates  $x$ ,  $y$ , and  $z$  of the vector pointing to the planet in the reference frame linked to the principal axes of inertia  $(\vec{f}_1, \vec{f}_2, \vec{f}_3)$ , from its coordinates in the inertial frame  $x_i$ ,  $y_i$  and  $z_i$ . Five rotations are to be performed:

$$\begin{pmatrix} x \\ y \\ z \end{pmatrix} = R_3(-l)R_1(-J)R_3(-g)R_1(-K)R_3(-h) \begin{pmatrix} x_i \\ y_i \\ z_i \end{pmatrix} \tag{A32}$$

with  $x_i$ ,  $y_i$ ,  $z_i$  depending on Io's orbital elements.

The rotation matrices are defined by

$$R_3(\phi) = \begin{pmatrix} \cos \phi & -\sin \phi & 0 \\ \sin \phi & \cos \phi & 0 \\ 0 & 0 & 1 \end{pmatrix}, \quad R_1(\phi) = \begin{pmatrix} 1 & 0 & 0 \\ 0 & \cos \phi & -\sin \phi \\ 0 & \sin \phi & \cos \phi \end{pmatrix}. \tag{A33}$$

The gravitational potential then reads:

$$V_1(l, g, h, J, K) = -\frac{3}{2}C \frac{\mathcal{G}M_{\text{J}}}{d^3} (\epsilon_1(x^2 + y^2) + \epsilon_2(x^2 - y^2)) \quad (\text{A34})$$

where  $\mathcal{G}$  is the gravitational constant,  $M_{\text{J}}$  the mass of the perturber Jupiter,  $(x, y, z)$  the vector pointing at Jupiter in the frame  $(\vec{f}_1, \vec{f}_2, \vec{f}_3)$ , while  $d$  is the distance planet-satellite.

From the variables  $x$ ,  $y$  and  $z$ , it is easy to introduce the set of variables defined in (Eq. A29), and we get:

$$\mathcal{H}_2(p, P, r, R, \xi_1, \eta_1) = -\frac{3}{2} \frac{\mathcal{G}M_{\text{J}}}{nd^3} (\epsilon_1(x^2 + y^2) + \epsilon_2(x^2 - y^2)). \quad (\text{A35})$$

Finally, we use the formulae (A30) and (A35) to get the Hamiltonian of the system:

$$\mathcal{H} = \mathcal{H}_1(P, \xi_1, \eta_1, \xi_2, \eta_2) + \mathcal{H}_2(p, P, r, R, \xi_1, \eta_1). \quad (\text{A36})$$

The four degrees of freedom of this Hamiltonian are the spin  $(p, P)$ , the obliquity  $(r, R)$ , the wobble of the whole body  $(\xi_1, \eta_1)$  and the wobble of the core  $(\xi_2, \eta_2)$ .

## B. The NAFF algorithm

The frequency analysis algorithm that we use is based on Laskar’s original idea, named NAFF as Numerical Analysis of the Fundamental Frequencies (see for instance Laskar (1993) for the method, and Laskar (2005) for the convergence proofs). It aims at identifying the coefficients  $a_k$  and  $\omega_k$  of a complex signal  $f(t)$  obtained numerically over a finite time span  $[-T; T]$  and verifying

$$f(t) \approx \sum_{k=1}^n a_k \exp(i\omega_k t), \quad (\text{B1})$$

where  $\omega_k$  are real frequencies and  $a_k$  complex coefficients. If the signal  $f(t)$  is real, its frequency spectrum is symmetric and the complex amplitudes associated with the frequencies  $\omega_k$  and  $-\omega_k$  are complex conjugates. The frequencies and amplitudes associated are found with an iterative scheme. To determine the first frequency  $\omega_1$ , one searches for the maximum of the amplitude of

$$\phi(\omega) = \langle f(t), \exp(i\omega t) \rangle, \quad (\text{B2})$$

where the scalar product  $\langle f(t), g(t) \rangle$  is defined by

$$\langle f(t), g(t) \rangle = \frac{1}{2T} \int_{-T}^T f(t) g(t)^* \chi(t) dt, \quad (\text{B3})$$

$g(t)^*$  being the complex conjugate of  $g(t)$ .  $\chi(t)$  is a weight function alike a Hann or a Hamming window, i.e. a positive function verifying

$$\frac{1}{2T} \int_{-T}^T \chi(t) dt = 1. \quad (\text{B4})$$

Using such a window can help the determination in reducing the amplitude of secondary minima in the transform (B3). Its use is optional.

Once the first periodic term  $\exp(i\omega_1 t)$  is found, its complex amplitude  $a_1$  is obtained by orthogonal projection, and the process is started again on the remainder  $f_1(t) = f(t) - a_1 \exp(i\omega_1 t)$ . The algorithm stops when two detected frequencies are too close to each other, what alters their determinations, or when the number of detected terms reaches a limit set by the user. This algorithm is very efficient, except when two frequencies are too close to each other. In that case, the algorithm is not confident in its accuracy and stops. When the difference between two frequencies is larger than twice the frequency associated with the length of the total time interval, the determination of each fundamental frequency is not perturbed by the other ones. Although an iterative method suggested by Champenois (1998) allows to reduce this distance, some troubles may remain. In our peculiar case of the Poincaré-Hough model applied to Io, these problems are likely to arise because of the proximity between the free frequency of the core  $\omega_z$  and the frequency of the spin.

## REFERENCES

- Anderson J.D., Sjogren W.L. & Schubert G., 1996, Galileo gravity results and the internal structure of Io, *Science*, 272, 709-712
- Anderson J.D., Jacobson R.A., Lau E.L., Moore W.B. & Schubert G., 2001, Io's gravity field and interior structure, *J. Geophys. Res.*, 106, 32,963-32,969
- Andoyer H., 1926, *Mécanique Céleste*, Gauthier-Villars, Paris
- Archinal B.A., A'Hearn M.F., Howell E., Conrad A., Consolmagno G.J., Courtin R., Fukushima T., Hestroffer D., Hilton J.L., Krasinsky G.A., Neumann G., Oberst J., Seidelmann P.K., Stooke P., Tholen D.J., Thomas P.C. & Williams I.P., 2011, Report

- of the IAU Working Group on cartographic coordinates and Rotational Elements: 2009, *Celestial Mechanics and Dynamical Astronomy*, 109, 101-135
- Bayly B.J., 1986, Three-dimensional instability of elliptical flow, *Phys. Rev. Lett.*, 57, 2160-2163
- Bouquillon S., Kinoshita H. & Souchay J., 2003, Extension of Cassini's laws, *Celestial Mechanics and Dynamical Astronomy*, 86, 29-57
- Cassen P.M., Peale S.J. & Reynolds R.T., 1982, Structure and thermal evolution of the Galilean satellites, in : *Satellites of Jupiter*, D. Morrison ed., 93-128, University of Arizona Press, Tucson
- Cassini G.D., 1693, *Traité de l'origine et du progrès de l'astronomie*, Paris
- Cebon D., Le Bars M., Moutou C. & Le Gal P., 2012, Elliptical instability in terrestrial planets and moons, *A&A*, 539, A78
- Champanois S., 1998, Dynamique de la résonance entre Mimas et Téthys, premier et troisième satellites de Saturne, Ph.D. Dissertation, Observatoire de Paris, in French
- Colombo G., 1966, Cassini's second and third laws, *AJ*, 71, 891-896
- De Haerdtl E., 1892, Sur une inégalité du quatrième ordre provenant de l'action mutuelle des deux derniers satellites de Jupiter, *Bulletin Astronomique*, 9, 212-216, in French
- de Pater I. & Lissauer J.J., 2010, *Planetary Sciences*, Second Edition, Cambridge University Press, New York
- Dufey J., Lemaître A. & Rambaux N., 2008, Planetary perturbations on Mercury's libration in longitude, *Celestial Mechanics and Dynamical Astronomy*, 101, 141-157
- Gladman B., Quinn D.D., Nicholson P. & Rand R., 1996, Synchronous locking of tidally evolving satellites, *Icarus*, 122, 166-192
- Goldreich P. & Peale S.J., 1966, Spin-orbit coupling in the solar system, *AJ*, 71, 425-438
- Greenspan H.P. & Howard L.N., 1963, On a time-dependent motion of a rotating fluid, *Journal of Fluid Mechanics*, 17, 385-404
- Henrard J., 2005, The rotation of Io, *Icarus*, 178, 144-153
- Henrard J., 2008, The rotation of Io with a fluid core, *Celestial Mechanics and Dynamical Astronomy*, 101, 1-12

- Herreman W., Le Bars M. & Le Gal P., 2009, On the effects of an imposed magnetic field on the elliptical instability in rotating spheroids, *Physics of Fluids*, 21, 046602
- Hough S.S., 1895, The oscillations of a rotating ellipsoidal shell containing fluid, *Philosophical transactions of the Royal Society of London A*, 186, 469-506
- Jeffreys H., 1976, *The Earth. Its origin, history and physical construction*, 6th edition, Cambridge University Press, Cambridge
- Kerswell R.R. & Malkus W.V.R., 1998, Tidal instability as the source for Io's magnetic signature, *Geophys. Res. Lett.*, 25, 603-606
- Kerswell R.R., 2002, Elliptical instability, *Annual Review of Fluid Mechanics*, 34, 83-113
- Lainey V., Duriez L. & Vienne A., 2006, Synthetic representation of the Galilean satellites' orbital motions from L1 ephemerides, *A&A*, 456, 783-788
- Lainey V., Arlot J.E., Karatekin Ö. & Van Hoolst T., 2009, Strong tidal dissipation in Io and Jupiter from astrometric observations, *Nature*, 459, 957-959
- Laskar J., 1993, Frequency analysis of a dynamical system, *Celestial Mechanics and Dynamical Astronomy*, 56, 191-196
- Laskar J., 2005, Frequency map analysis and quasiperiodic decompositions, in *Hamiltonian systems and fourier analysis: new prospects for gravitational dynamics*, Benest et al. editors, Cambridge Sci. Publ., 99-129
- Lieske J.H., 1973, On the 3-7 commensurability between Jupiter's outer two Galilean satellites, *A&A*, 27, 59-65
- Margot J.-L., Peale S.J., Jurgens R.F., Slade M.A. & Holin I.V., 2007, Large longitude libration of Mercury reveals a molten core, *Science*, 316, 710-714
- Noyelles B. & Vienne A., 2007, Chaos induced by De Haerdtl inequality in the Galilean system, *Icarus*, 190, 594-607
- Noyelles B., 2008, Titan's rotational state: The effects of a forced "free" resonant wobble, *Celestial Mechanics and Dynamical Astronomy*, 101, 13-30
- Noyelles B., Dufey J. & Lemaitre A., 2010, Core-mantle interactions for Mercury, *MNRAS*, 407, 479-496
- Noyelles B., Karatekin Ö. & Rambaux N., 2011, The rotation of Mimas, *A&A*, 536, A61

- Noyelles B., 2012, Behavior of nearby synchronous rotation of a Poincaré-Hough satellite at low eccentricity, *Celestial Mechanics and Dynamical Astronomy*, in press, doi:10.1007/s10569-012-9398-y
- Noyelles B., Delsate N. & Carletti T., Equilibrium search algorithm of a perturbed quasi-integrable system: NAFFO – Numerical Algorithm For Forced Oscillations, submitted, arXiv:1101.2138
- Peale S.J., Cassen P. & Reynolds R.T., 1979, Melting of Io by tidal dissipation, *Science*, 203, 892-894
- Peale S.J., Margot J.L. & Yseboodt M., 2009, Resonant forcing of Mercury’s libration in longitude, *Icarus*, 199, 1-8
- Pierrehumbert R.T., 1986, Universal short-wave instability of two-dimensional eddies in an inviscid fluid, *Phys. Rev. Lett.*, 57, 2157-2159
- Poincaré H., 1910, Sur la précession des corps déformables, *Bulletin Astronomique*, 27, 321-357
- Rambaux N., Castillo-Rogez J.C., Williams J.G. & Karatekin Ö., 2010, Librational response of Enceladus, *Geophys. Res. Lett.*, 37, L04202
- Touma J. & Wisdom J., 2001, Nonlinear core-mantle coupling, *The Astronomical Journal*, 122, 1030-1050
- Usselman T.M., 1975, Experimental approach to the state of the core; Part I, The liquidus relations of the Fe-rich portion of the Fe-Ni-S system from 30 to 100 kb, *American Journal of Science*, 275, 278-290
- Van Hoolst T., Rambaux N., Karatekin Ö., Dehant V. & Rivoldini A., 2008, The librations, shape, and icy shell of Europa, *Icarus*, 195, 386-399
- Williams J.G., Boggs D.H., Yoder C.F., Ratcliff J.T. & Dickey J.O., 2001, Lunar rotational dissipation in solid body and molten core, *J. Geophys. Res.*, 106, 27,933-27,968
- Yseboodt M., Margot J.-L. & Peale S.J., 2010, Analytical model of the long-period forced longitude librations of Mercury, *Icarus*, 207, 536-544

## List of Figures

1	Variations of the keplerian elements of Io, as given by the theory L1.2 Lainey et al. (2006). . . . .	10
2	In the upper panel we have 3 reference frames: one linked to the ecliptic plane ( $\vec{e}_1, \vec{e}_2, \vec{e}_3$ ), another linked to the angular momentum $\vec{G}$ ( $\vec{n}_1, \vec{n}_2, \vec{n}_3$ ), and the last one linked to the axes of inertia ( $\vec{f}_1, \vec{f}_2, \vec{f}_3$ ) of the satellite. In the lower panel we have a similar configuration but instead of the angular momentum of the satellite, we have a reference frame linked to the angular momentum of a pseudo-core . . . . .	13
3	The four reference frames gathered in the same view. The angles ( $h, K$ ) position the plane orthogonal to the angular momentum $\vec{N}$ . The Euler angles ( $g, J, l$ ) locate the axis of least inertia and the body frame ( $\vec{f}_1, \vec{f}_2, \vec{f}_3$ ). The angles ( $J_c, l_c$ ) place the angular momentum of the pseudo-core with respect to the axis of least inertia $f_1$ . . . . .	14
4	Observable outputs of the Model 1 (core made of pure iron). . . . .	20
5	Observable outputs of the Model 2 (core made of FeS). . . . .	23
6	Expected longitudinal librations. . . . .	24
7	Growth rate in the model 1. . . . .	27

## List of Tables

1	Gravity and shape parameters of Io. . . . .	3
2	Physical parameters of our 10 models. . . . .	8
3	Parameters required by the Poincaré-Hough model. . . . .	9
4	Proper modes of the orbital dynamics of the Galilean satellites of Jupiter, given by Lainey et al. (2006). With all these modes, the orbits of the Galilean satellites can be reconstructed. The phases are given at J2000.0=JD 2451545. . . . .	11
5	Free or proper frequencies $\omega$ and the periods associated $T$ for the 10 models of Io. . . . .	18
6	Frequency analysis of the longitudinal librations $\phi_m$ , in the Model 1. The series are in sine. . . . .	21

7	Frequency analysis of the obliquity of the mantle $\epsilon_m$ , in the Model 1. The series are in cosine. . . . .	21
8	Frequency analysis of the amplitude of the polar motion of the mantle $J_m$ , in the Model 1. The series are in cosine. . . . .	22
9	Frequency analysis of the amplitude of the tilt of the fluid $J_c$ , in the Model 1. The series are in cosine. . . . .	22
10	Variations of the outputs in the different models. . . . .	25
11	Parameters used to compute the grow rate $\sigma$ . . . . .	26
12	Mean grow rate $\langle \sigma \rangle$ , and the time associated compared with the spin-up time $t_{spin-up}$ . . . . .	28